12-2002

Residual Stress Effects on Fatigue Life via the Stress Intensity Parameter, K

Jeffrey Lynn Roberts
University of Tennessee - Knoxville

To the Graduate Council:

I am submitting herewith a dissertation written by Jeffrey Lynn Roberts entitled "Residual Stress Effects on Fatigue Life via the Stress Intensity Parameter, K." I have examined the final electronic copy of this dissertation for form and content and recommend that it be accepted in partial fulfillment of the requirements for the degree of Doctor of Philosophy, with a major in Engineering Science.

John D. Landes, Major Professor

We have read this dissertation and recommend its acceptance:

J. A. M. Boulet, Charlie R. Brooks, Niann-i (Allen) Yu

Accepted for the Council:

Carolyn R. Hodges

Vice Provost and Dean of the Graduate School

(Original signatures are on file with official student records.)

To the Graduate Council:

I am submitting herewith a dissertation written by Jeffrey Lynn Roberts entitled "Residual Stress Effects on Fatigue Life via the Stress Intensity Parameter, K." I have examined the final electronic copy of this dissertation for form and content and recommend that it be accepted in partial fulfillment of the requirements for the degree of Doctor of Philosophy, with a major in Engineering Science.

John D. Landes

Major Professor

We have read this dissertation
and recommend its acceptance:

J. A. M. Boulet

Charlie R. Brooks

Niann-i (Allen) Yu

Accepted for the Council:

Anne Mayhew
Vice Provost and Dean of
Graduate Studies

(Original signatures are on file with official student records.)

Residual Stress Effects on Fatigue Life via the Stress Intensity Parameter, K

A Dissertation
Presented for the
Doctor of Philosophy Degree
The University of Tennessee, Knoxville

Jeffrey L. Roberts
December 2002

Dedication

This dissertation is dedicated to my wife, Laila, my daughter, Samara, and my son, Yusef. Their love and support have provided me the inspiration and the motivation necessary for such an endeavor.

Acknowledgements

Completion of this dissertation research has required the time, resources and support of many people. I am greatly indebted to my advisor and committee chairman, Dr. John D. Landes, for his continuous support and guidance. Without his advice and generosity of time, this work would not have been possible. I am also grateful to Dr. Charlie R. Brooks, Dr. J. A. M. Boulet and Dr. Niann-i (Allen) Yu for serving as members of my doctoral committee, and for their patience with my perpetually changing schedule.

Special thanks are also due my employer, Saturn Corporation, for supporting me with a reduced work schedule during this effort. Without the cooperation and support of management and my fellow team members, this research could not have been completed.

Abstract

Residual stresses are known to have a significant effect on fatigue crack propagation and thus fatigue life. These effects have generally been quantified through an empirical approach, lending little help in the quantitative prediction of such effects. The weight function method has been used as a quantitative predictor, but its use neglects residual stress redistribution, treating the residual stress as a constant during crack growth. At least three different behaviors contribute to the redistribution of residual stress. First, the residual stress behind the crack tip is reduced to a negligible level as soon as the crack tip passes. Second, the residual stress tends to redistribute away from the crack tip with crack growth, and third, crack growth results in an overall relaxation of residual stress.

An alternative method for predicting the effect of a residual stress distribution on fatigue crack growth is herein developed. The stress intensity factor due to residual stress, $K_{res,}$ is characterized as the change in crack driving force due to the presence of the residual stress. This crack driving force, being the derivative of a potential, is found through superposition of an applied stress and a residual stress, and subsequent manipulation of finite element strain energy and nodal displacement results.

Finite element modeling is carried out using a spatial distribution of non-uniform thermal expansion coefficients and a unit temperature load to simulate the desired residual stress. Crack growth is then achieved through use of a node release algorithm which sequentially removes nodal displacement constraint. The complete stress distribution, nodal displacements and internal strain energy are captured for each increment of

crack growth, and from this information, knowledge of the stress intensity factor as a function of crack length is derived.

Results of the K_{res} calculations are used in a fatigue crack growth model to predict fatigue lives. The fatigue life model involves step by step analysis of crack growth increment based on knowledge of stress intensity factors resulting from applied and residual stress. The qualitative effects of residual stress predicted by this model agree with documented empirical results which show that compressive residual stress increases fatigue life, while tensile residual stress decreases fatigue life.

Two solutions for K_{res} are possible, depending on the choice of load-control or displacement-control modeling. Use of displacement-control, or fixed displacement loading, minimizes redistribution of residual stress and, under net tensile loading, tends to lead to more conservative fatigue life predictions. Load-control modeling, not having the same displacement constraint, allows more relaxation of the residual stress and tends to provide the more non-conservative life estimates.

Three residual stress patterns, two due to welding and one to shot peening, are also investigated. K_{res} solutions for each residual stress are developed, and fatigue life predictions made. Regression analyses on the parameters defining the residual stress patterns indicate that, within the range specified for these parameters, the residual stress half-width plays a significant role in fatigue life, while the initial stress amplitude may be of less importance.

The conclusions reached in this research are as follows: The effect of residual stress on fatigue life can be quantified by the energy methods detailed herein. Weight function methods for predicting fatigue lives fail to

account for residual stress redistribution, which can have a significant effect. Knowledge of K_{res} allows subsequent predictions of fatigue life via a simple superposition of applied and residual stress intensity factors, and enables further investigation of relevant residual stress parameters and their effects. The ability to analytically vary residual stress parameters and quantify their effects on fatigue life could prove to be a significant design aid. Based on these conclusions, it is recommended that further development of the energy methods, as presented here, be pursued.

Contents

List of Figures

List of Tables

List of Symbols and Acronyms

a	(a) Crack Length
	(b) Ellipse Major Axis
	(c) Fitting Constant
a_{eff}	Effective Crack Length
a_f	Final Crack Length
a_{ij}	Thermal Expansion Coefficient Matrix
a_0	Initial Crack Length
b	(a) Ellipse Minor Axis
	(b) Empirically Derived Regression Parameter
	(c) Masubuchi Residual Stress Field Half-Width
c	Empirically Derived Regression Parameter
d	Atomic Spacing (Bragg Law)
dA	Incremental Crack Surface Area
da/dN	Crack Growth per Load Cycle
ds	Differential Element of Contour Path Γ
e_{pkl}	Permutation Symbol
f_{ij}	Dimensionless Function of θ
$h(x)$	Weight Function
i	Imaginary Number $\sqrt{-1}$
k_t	Stress Concentration Factor
m	Empirically Derived Power Law Exponent

m_1	Empirically Derived Power Law Exponent (R=0 case)
n	Integer
n'	Fitting Constant for Strain-Hardening Constitutive Equation
n_j	Normal Vector
r	Distance from Crack Tip
r_c	Current Plastic Zone Size (Wheeler)
r_y	Plastic Zone Size
u^*	Approximation to True Displacement Field
$\{u\}$	Displacement Vector
w	Strain Energy Density
A	Empirically Derived S-N Regression Parameter
A_m	General Elastic Solution Expansion Coefficients
B	(a) Specimen Thickness (b) Empirically Derived Regression Parameter
B_i	Body Force Vector
C	Empirically Derived Regression Parameter
C_1	Empirically Derived Regression Parameter (R=0 case)
D	Empirically Derived Regression Parameter
D_{ijkl}	Stress-Strain Constitutive Coefficient Matrix
$[D]$	Partial Differential Operator
E	Young's Modulus
E'	Effective Young's Modulus

$[E]$	Elastic Coefficient Matrix
F	Work Done by External Loading
G	Energy Release Rate for Linear Elastic Material Behavior
H'	Fitting Constant for Strain-Hardening Constitutive Equation
Im	Imaginary Part of Complex Expression
J	Energy Release Rate for Nonlinear Material Behavior
K_{app}	Stress Intensity Factor due to Applied Mechanical Load
K_c	Critical Stress Intensity (Forman Equation)
K_{eff}	Effective Stress Intensity Factor
K_I	Mode I Stress Intensity Factor
K_{Ic}	Critical Mode I Stress Intensity Factor
K_{min}	Minimum Stress Intensity during Load Cycle
K_{max}	Maximum Stress Intensity during Load Cycle
$K_{min\_applied}$	Minimum Stress Intensity Factor due to Applied Mechanical Loading
$K_{max\_applied}$	Maximum Stress Intensity Factor due to Applied Mechanical Loading
K_{op}	Crack Face Opening Stress Intensity Factor
K_{res}	Stress Intensity Factor due to Residual Stress
K_{tot}	Total Stress Intensity Factor
$[K]$	Stiffness Matrix

M	Bending Moment
N	Number of Cycles to Grow from a_0 to a_f
N_f	Number of Load Cycles to Failure
$N_f{}^0$	Number of Load cycles to Failure w/out Residual Stress
N_t	Transition Fatigue Life
P_i	External Load on Node 'i'
Q_α	Expansion Coefficients in Weak Statement Approximation
R	Load Ratio
Re	Real Part of Complex Expression
R_{pq}	Strain Compatibility Equations (Indicial Notation)
$\{R\}$	Residual Data
S_a	Section Average Stress Amplitude
S_m	Mean Nominal Stress
S_{max}	Maximum Net Section Stress
T_i	Traction Vector
U	(a) Internal Strain Energy (b) Ratio of Effective SIF Range and SIF Range
$\{U\}$	Displacement Field
W	Specimen Width
$WS*$	Weak Statement Approximation
X, Y, Z	Untransformed Cartesian Coordinates

α	(a) Plastic Zone Parameter
	(b) Strain Gage Orientation Angle
α_n	Generic Thermal Expansion Coefficient
β	Strain Gage Orientation Angle
δ_e	Equilibrium Displacement
ε_a	(a) Cyclic Strain Amplitude
	(b) Strain Rosette Measurement
$\varepsilon_b, \varepsilon_c$	Strain Rosette Measurements
ε_e	Elastic Strain
ε'_f	Empirically Derived Regression Parameter
ε_p	Plastic Strain
$\varepsilon_x, \varepsilon_y, \varepsilon_{xy}$	Strain Tensor Components
$\varepsilon_{x'}, \varepsilon_{y'}, \varepsilon_{x'y'}$	Strain Tensor Components Transformed to (X', Y')
	Coordinate System
ε_{ij}^{e}	Elastic Strain Tensor
ε_{ij} *	Eigenstrain Tensor
$\varepsilon *_{ij,kl}$	Partial Derivative Notation of Eigenstrain Components
$\{\varepsilon\}$	Small Strain Vector
ϕ	Green's Function
ϕ_R	Wheeler Retardation Factor
γ	(a) Fitting Parameter
	(b) Strain Gage Orientation Angle

η	Finite Element Parametric Coordinate
λ	Wavelength of Incident Radiation (Bragg's Law)
θ	(a) Polar Coordinate in Crack Tip Coordinate System (b) Angle of Coordinate System Rotation for Strain Transformation Equations (c) Angle Between Incident Beam and Atomic Planes in Bragg's Law
ρ	Elliptic Curvature as Defined by Inglis
σ_a	Cyclic Stress Amplitude
σ'_f	Empirically Derived Regression Parameter
σ_{ij}	Stress Tensor
σ_r	Masubuchi Residual Stress
σ_{res}	Residual Stress
σ_{res}^{i}	Initial Residual Stress
σ_{res}^{R}	Redistributed Residual Stress
$\sigma_{xx}, \sigma_{yy}, \sigma_{xy}$	Stress Tensor Components
σ_{ys}	Yield Stress
υ	Poisson Ratio
ξ	Finite Element Parametric Coordinate
ζ	Finite Element Parametric Coordinate
Δ	General Displacement Notation
Δ_i	Nodal Displacement of Node 'i'

Δ_h	Finite Element Mesh Dimension
ΔJ	Nonlinear Stress Intensity Factor Range
ΔK	Stress Intensity Factor Range
$\Delta \overline{K}$	Equivalent Zero to Tension SIF Range
ΔK_{th}	Threshold Stress Intensity Factor Range
$\Delta \overline{S}$	Equivalent Zero to Tension Mean Stress Range
Φ	Airy Stress Function
Γ	General Contour Path
Γ_c	Crack Perimeter
Π	Potential Energy of an Elastic Body
Ψ_α	Trial Space in Weak Statement Approximation
∇^2	Laplacian Operator
CTOD	**C**rack **T**ip **O**pening **D**isplacement
FCG	**F**atigue **C**rack **G**rowth
FEA	**F**inite **E**lement **A**nalysis
FEM	**F**inite **E**lement **M**odel
GWS	**G**alerkin **W**eak **S**tatement
LEFM	**L**inear **E**lastic **F**racture **M**echanics
SENT	**S**ingle **E**dge **N**otch **T**ension (Specimen)
SIF	**S**tress **I**ntensity **F**actor

Chapter 1

Introduction

The discipline of fracture mechanics has been born of an economic as well as public safety need. An economic study by Duga et al. [1] estimated the cost of fracture in the United States for the year 1978 to be 119 billion (adjusted for inflation to 1982 dollars), or 4% of that year's gross national product. More importantly, the human cost of failed structures has been documented throughout history by incidents ranging from airline disasters to catastrophic bridge and building collapse. Bannerman and Young [2] point out that fracture mechanics as a unique and serious scientific discipline however, was essentially non-existent prior to the Liberty ship failures of World War II. Since World War II, the body of information comprising fracture mechanics has grown to include the established fundamentals of linear elastic fracture involving the stress intensity factor (K), crack tip plasticity corrections for mildly nonlinear behavior, nonlinear parameter development for large-scale plasticity including J-integral and CTOD (crack tip opening displacement), and application to practical areas of engineering concern such as fatigue crack growth and component life prediction. The focus of this proposed research, as will be further detailed, is confined to the later.

The classic stress-based and strain-based engineering approaches to fatigue have been formulated to provide a prediction of the time (or number of cycles) until an observable (or measurable) flaw appears. These approaches have the disadvantage of considering only the time to initiation of a flaw as the useful life of the given component. Classic stress-based and

strain-based approaches both suffer from this shortcoming since, in many cases, the majority of the useful life of a component or structure consists of the growth stage of the initial flaw to its final or critical state. The fracture mechanics approach, on the other hand, considers only that part of the component life after the initiation of a defect or flaw.

In the 1960's, Paris [3, 4] demonstrated the usefulness of linear elastic fracture mechanics (LEFM) in characterizing fatigue crack growth. Paris determined that a relationship existed between the crack extension per load cycle and the range of the applied stress intensity factor, ΔK. The form of this relationship is a power law form and is today widely known as the Paris Law. In theory, application of this law to a fatigue crack growth problem can be performed, given enough information, to approximately predict the number of cycles until a critical flaw size is reached. The Paris Law served as a basis for the construction of more complicated laws which have attempted to account for threshold, crack closure, stress ratio and other effects. A typical (schematic) fatigue crack growth curve is shown in figure 1.1. This curve indicates the three regions of fatigue crack growth. Region I is the region in which little or no crack growth occurs due to the low value of stress intensity factor range. Region II indicates a power law relationship of the Paris Law type. Region III is a region of rapid crack propagation and imminent fracture.

While the above-mentioned fatigue crack growth (FCG) models have proven extremely useful for general and rough life estimates, there are situations in which their application is not straight-forward, and possibly not appropriate. History effects can violate some of the basic assumptions underlying these models, thus invalidating their predictions. More complex

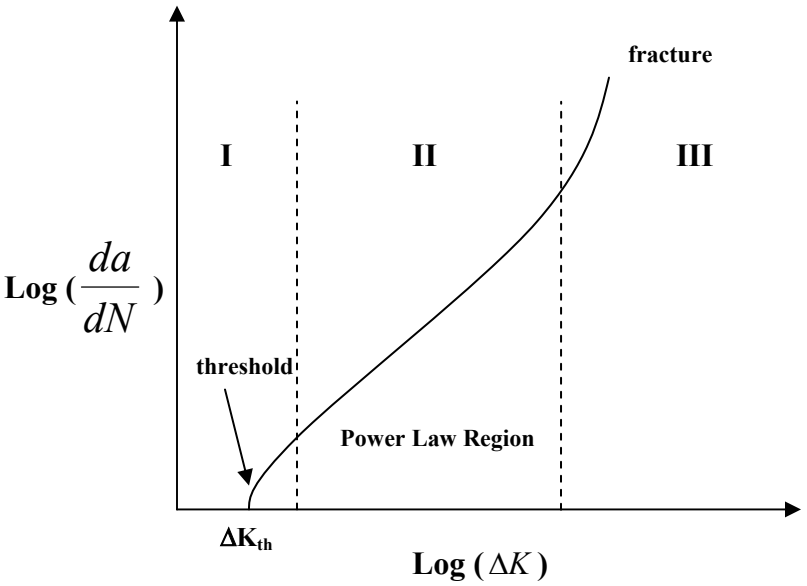

Figure 1.1: Schematic Fatigue Crack Growth Curve

models are required to account for a non-constant ΔK, such as in random loading, and for effects such as residual stress fields induced by overloading, welding, heat treatment or other thermal and/or mechanical processes. It is precisely these residual stress fields and their interaction with a fatigue crack which serve as motivation for the current research.

In the following chapters, the fundamentals of LEFM are discussed. The idea of stress intensity factor, K, is developed from a basic knowledge of stress concentrations. The mathematical foundations for linear elastic fracture are explained, and alternate solution methodologies for finding K, including finite element methods, are presented. The classic as well as fracture mechanics approaches to fatigue life estimation are described in an effort to build an understanding of current methods of fatigue life prediction. Shortcomings of the current fracture mechanics based fatigue models are explained, and the general problem of a fatigue crack growing through a residual stress field is detailed. Previous research efforts surrounding the effects of residual stress on K, although somewhat limited, are summarized, and a detailed explanation of recently conducted new research is presented. The focus of this new research is on using finite element modeling to develop quantitative models which more accurately describe the fatigue crack/residual stress field interaction.

Chapter 2

Linear Elastic Fracture Mechanics

In this chapter, the fundamentals of linear elastic fracture mechanics are reviewed. The fracture mechanics triangle is first explained, and the concept of stress concentrations is introduced. Formulation of the stress intensity factor (K) is then presented along with methods for obtaining solutions in closed form. A brief overview of classic finite element methods is also presented with an emphasis on derivation of the fundamental matrix statement. The energy approach to determining fracture mechanics parameters is then briefed, and finally, the limitations of LEFM are reviewed.

2.1 Fracture Mechanics Triangle

The classic approach to structural design and material selection typically involves stress analysis, with yield or tensile strength of the material being the limiting criteria. If the anticipated service stresses on the structure are less than the strength of the material, the material is assumed to be adequate. This approach assumes a homogeneous and defect-free material and its only protection against brittle fracture is based upon implementation of a safety factor on stress and/or ductility requirements on the material. The fracture mechanics approach, however, as illustrated by Anderson [5], relies on quantification of three critical variables: applied stress, fracture toughness and flaw size. These three critical variables comprise what is commonly referred to as the fracture mechanics triangle. Figure 2.1 provides a

(a) Classic Approach

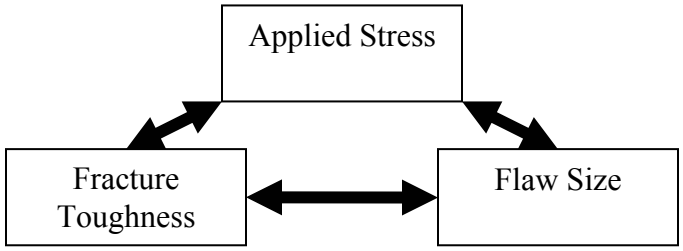

(b) Fracture Mechanics Approach

Figure 2.1: Comparison of Classic and Fracture Mechanics Design Approaches [5]

comparison of the classic and fracture mechanics approaches to structural design.

2.2 Stress Concentrations

One of the first quantitative analyses of the effect of stress concentration at a flaw was produced by Inglis [6]. Inglis' analysis was on elliptic holes in flat plates. With applied stress perpendicular to the major axis, as in figure 2.2, Inglis assumed that the hole itself was not influenced by the plate boundary. Considering the local stress at point 'A' of figure 2.2, Inglis found it convenient to express this stress as

$$\sigma_A = \sigma\left(1 + 2\sqrt{\frac{a}{\rho}}\right) \tag{2.1}$$

where

$$\rho = \frac{b^2}{a} \tag{2.2}$$

Inglis' results predict an infinite stress at the tip of a sharp crack, where $\rho \to 0$. This result led to serious concerns as to the validity of the findings since no material is capable of withstanding even an infinitesimal applied stress if it contains a sharp crack. Today, it is understood that a "sharp" crack is a mathematical abstraction since the minimum possible radius of a crack is on the order of the material's atomic radius. Furthermore, it is well established that initially sharp cracks tend to blunt themselves in a redistribution of stress caused by plastic flow in the immediate region of the crack tip. While equation (2.1) is not completely accurate in predicting realistic stress levels around sharp cracks, it does suggest one of the later,

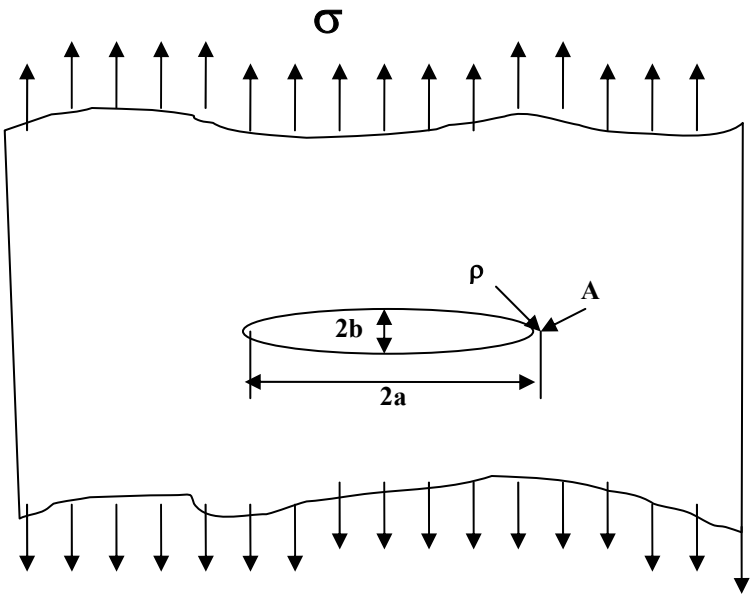

Figure 2.2: Elliptic Hole in a Flat Plate

well-established, characteristics of crack-tip stress fields. That important characteristic is the $1/\sqrt{r}$ crack-tip singularity, which is discussed in the next section.

2.3 Stress Intensity Factors

The concept of K as a stress intensity factor forms the basis of linear elastic fracture mechanics. Forthcoming formulations of K provide a mathematical description of the distribution of stresses near the tip of a crack, and give insight into the physical meaning of K. The following development shows how K is actually the amplitude of the crack tip stress singularity, and that if K is known, the complete distribution of stress near the crack tip can be found.

2.3.1 Closed Forms

If linear elastic, isotropic material behavior is assumed, closed-form solutions for the stresses in a cracked body are possible. One of the earliest published solutions was by Westergaard [7]. Westergaard treated a limited class of problems by introducing a complex stress function, $Z(z)$, where $z = x + iy$, and $i = \sqrt{-1}$. Given the Airy stress function, defined as the function, $\Phi(x, y)$, which has the following properties

$$\Phi_x = \frac{\partial^2 \Phi}{\partial y^2}, \Phi_y = \frac{\partial^2 \Phi}{\partial x^2}, \tau_{xy} = \frac{\partial^2 \Phi}{\partial x \partial y}, \nabla^2 \nabla^2 \Phi = 0 \qquad (2.3)$$

Westergaard's complex stress function was defined as

$$\Phi = \mathrm{Re}\overline{\overline{Z}} + y\,\mathrm{Im}\,\overline{Z} \qquad (2.4)$$

where Re and Im denote real and imaginary parts of $Z(z)$, and the overbars represent integrations with respect to 'z' such that

$$Z = \frac{d\overline{Z}}{dz}, \text{ etc.} \tag{2.5}$$

The Westergaard approach leads to the expected $1/\sqrt{r}$ singularity, and complete analysis on a through-thickness crack in an infinite plate in biaxial tension yields

$$\begin{aligned}
\sigma_{xx} &= \frac{K_I}{\sqrt{2\pi r}}\cos\left(\frac{\theta}{2}\right)\left[1-\sin\left(\frac{\theta}{2}\right)\sin\left(\frac{3\theta}{2}\right)\right] \\
\sigma_{yy} &= \frac{K_I}{\sqrt{2\pi r}}\cos\left(\frac{\theta}{2}\right)\left[1+\sin\left(\frac{\theta}{2}\right)\sin\left(\frac{3\theta}{2}\right)\right] \\
\tau_{xy} &= \frac{K_I}{\sqrt{2\pi r}}\cos\left(\frac{\theta}{2}\right)\sin\left(\frac{\theta}{2}\right)\cos\left(\frac{3\theta}{2}\right)
\end{aligned} \tag{2.6}$$

Independent research by Irwin [8] and Sneddon [9] also produced closed-form results which showed the same general singularity characteristic. In general, if a polar coordinate system is defined with the origin at the crack tip, as in figure 2.3, it has been shown that the crack tip stress field in any elastic body with is given by

$$\sigma_{ij} = \left(\frac{k}{\sqrt{r}}\right) f_{ij}(\theta) + \sum_{m=1}^{\infty} A_m r^{\frac{m}{2}} g_{ij}^{(m)}(\theta) \tag{2.7}$$

where σ_{ij} is the stress tensor, r and θ are defined in figure 2.3, k is a constant and f_{ij} is a dimensionless function of θ. The terms in the summation depend on geometry, but all the terms vanish as $r \to 0$. The lead term, however, contains the $1/\sqrt{r}$ singularity and thus approaches

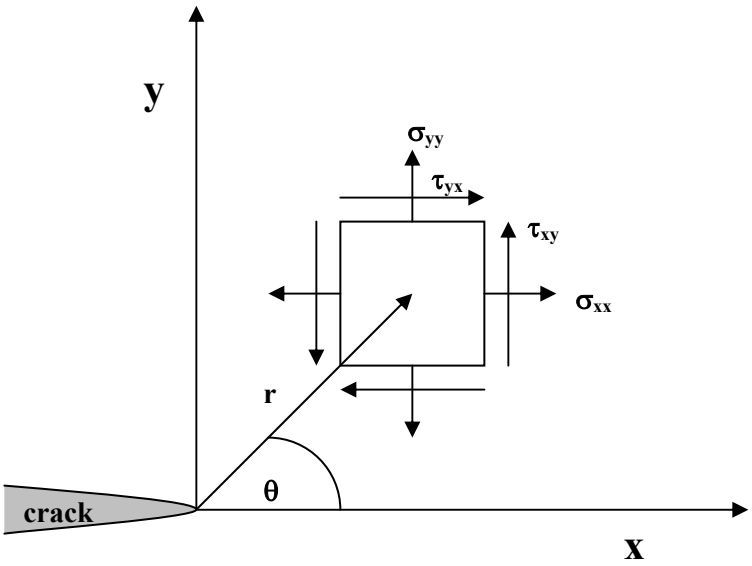

Figure 2.3: Definition of Coordinate Axes at Crack Tip

infinity in the limiting case where $r \to 0$. It is apparent, therefore, that the stress distribution near the crack tip varies with $1/\sqrt{r}$ regardless of the geometry of the cracked body.

Making the substitution for stress intensity factor, $K = k\sqrt{2\pi}$, into equation (2.7), the stress field near the tip of the crack can be written as

$$\lim_{r\to 0} \sigma_{ij}^{(I)} = \frac{K_I}{\sqrt{2\pi r}} f_{ij}^{(I)}(\theta) \tag{2.8}$$

where the 'I' notation denotes mode I loading. Thus, it is evident that the single parameter completely defining crack tip conditions is the stress intensity factor, K.

While useful calculation and inquiry can be performed with equations of the type obtained in closed form, it must be noted that the Westergaard approach assumes a semi-infinite body relative to the crack size, and this is often not the practical case. In order to find practical use in K, one must be able to determine, with some respectable accuracy, a good estimate of its value. In order to do this, the effects of finite size must be considered.

2.3.2 Finite Size Effects

As the flaw size becomes significant relative to the dimensions of the body, the outer boundaries of the body begin to have an influence on the crack tip. The net effect of finite geometry is a higher stress intensity surrounding the crack tip. Although there are limited closed-form solutions for such finite geometry problems, the most common and often most practical method for obtaining solutions is through numerical methods. Tada et al. [10] have published a wide range of both numerical and closed-form solutions in

handbook form. A primary tool for their numerical solutions is finite element methods. A brief overview of finite element methods will be presented in the next section as a prelude to the more specific and detailed discussions given later regarding specific techniques to be used in the current research.

2.3.3 Finite Element Method

The most common numerical method in use today for structural mechanics problems is the finite element method. Since the scope of the current research includes application of finite element methods to the direct problem of finding SIF solutions, as well as to understanding stress distributions and redistributions in the presence of a growing crack, inclusion of its basic principles is warranted within this discussion.

The benchmark two-dimensional structural mechanics problem comes from plate theory. This particular problem serves well the purpose of illustrating finite element basic principles. The applicable partial differential equation statement (for static load), as given by Baker [11], is Newton's law

$$\frac{\partial \sigma_{ij}}{\partial x_j} + B_i = 0 \tag{2.9}$$

where σ_{ij} is the stress tensor and B_i is the body force. Formulation of a Galerkin Weak Statement (GWS) on the above partial differential equation produces a matrix statement suitable for solution by common iterative techniques. Rewriting the above PDE in matrix form we have

$$\left[\mathrm{D}\right]^T \left\{\sigma\right\} + \left\{b\right\} = \left\{0\right\} \tag{2.10}$$

where

$$[D] = \begin{bmatrix} \dfrac{\partial}{\partial x} & 0 \\ 0 & \dfrac{\partial}{\partial y} \\ \dfrac{\partial}{\partial y} & \dfrac{\partial}{\partial x} \end{bmatrix} \tag{2.11}$$

Substituting $\{\sigma\} = [E]\{\varepsilon\}$, and $\{\varepsilon\} = [D]\{u\}$, where $\{u\} = \begin{Bmatrix} u \\ v \end{Bmatrix}$ is the displacement vector, we obtain the final matrix differential form for Newton's law as

$$[D]^T [E][D]\{u\} + \{b\} = \{0\} \tag{2.12}$$

Formation of the Weak Statement on the above matrix equation for any approximation defined as u^* results in

$$WS^* \equiv \int_{\Omega} \Psi_\alpha(x)\left([D]^T [E][D]\{u^*\} + \{b\}\right) d\tau \equiv 0 \tag{2.13}$$

for all $\Psi_\alpha(x)$, where $\Psi_\alpha(x)$ is the trial space function set to be used in the approximation,

$$u(x) \approx u^*(x) \equiv \sum_{\alpha}^{N} \Psi_\alpha(x) Q_\alpha \tag{2.14}$$

and Q_α are unknown expansion coefficients. Applying the Green-Gauss divergence theorem, as detailed by Baker [11], results in

$$WS^* = \int_{\Omega} \left[D\Psi_\alpha(x) \right]^T \left[E \right] \left[D \right] \left\{ u^* \right\} d\tau - \int_{\Omega} \Psi_\alpha(x) \left\{ b \right\} d\tau$$
$$- \oint_{\partial\Omega} \Psi_\alpha(x) \left(\left[D \right]^T \bullet \hat{n} \right) \left[E \right] \left[D \right] \left\{ u^* \right\} d\sigma \tag{2.15}$$

It must be noted that the functions $\Psi_\alpha(x)$ and $u^*(x)$ are functions of the vector $\{x\} = \begin{Bmatrix} x_1 \\ x_2 \end{Bmatrix}$, and not of the scalar value x. Equation (2.15) is the general weak statement form of the original partial differential equation (Newton's law). Further manipulation is required to form the weak statement on a single element, which is specific to element type. The assembly of all such elements then forms the global system of equations which must be solved for the displacements, $\{u^*\}$.

A second, and possibly less cumbersome, formulation can be constructed from the principles of virtual work. The derivation is based upon the integral form of potential energy. It is sufficient to say here that the variational virtual work formulation and the Galerkin Weak Statement written on the original PDE *exactly* reproduce one another. Thus, the general form of the resulting system of equations by either formulation is

$$\left[K \right] \left\{ U \right\} = \left\{ R \right\} \tag{2.16}$$

where $\left[K \right]$ is the stiffness matrix, $\left\{ U \right\}$ is the displacement field and $\left\{ R \right\}$ is the residual containing all known data such as boundary conditions, etc.

When singularities are present within the domain of interest, special care must be taken to insure that the solution generated by the finite element method will accurately represent the steep gradients present near the

singularity. In the case of a sharp crack, special elements have been developed which are convenient for this purpose. Figure 2.4 shows one such element which exhibits a $1/\sqrt{r}$ singularity. Here the triangular element is a collapsed quadrilateral element which is placed with the collapsed end at the crack tip.

In certain situations, however, the stress field near the crack tip may not be as important to the analyst as simply determining a fracture mechanics parameter such as the stress intensity factor. When this is the case, more convenient and easily implemented methods can be used. The following section develops the fundamentals of the energy approach to determination of fracture mechanics parameters.

2.3.4 The Energy Approach

Often, it is convenient to express the concept of a growing crack in terms of an energy release rate. Irwin [12] proposed that the energy release per unit increase in crack surface area was simply the change in potential energy of the body, expressed as

$$G = -\frac{d\Pi}{dA} \tag{2.17}$$

where Π is the potential energy of the body, and G is the energy release per unit area. With this definition of the energy release rate concept, it can be shown that the linear elastic stress intensity factor, K, is related to G as follows:

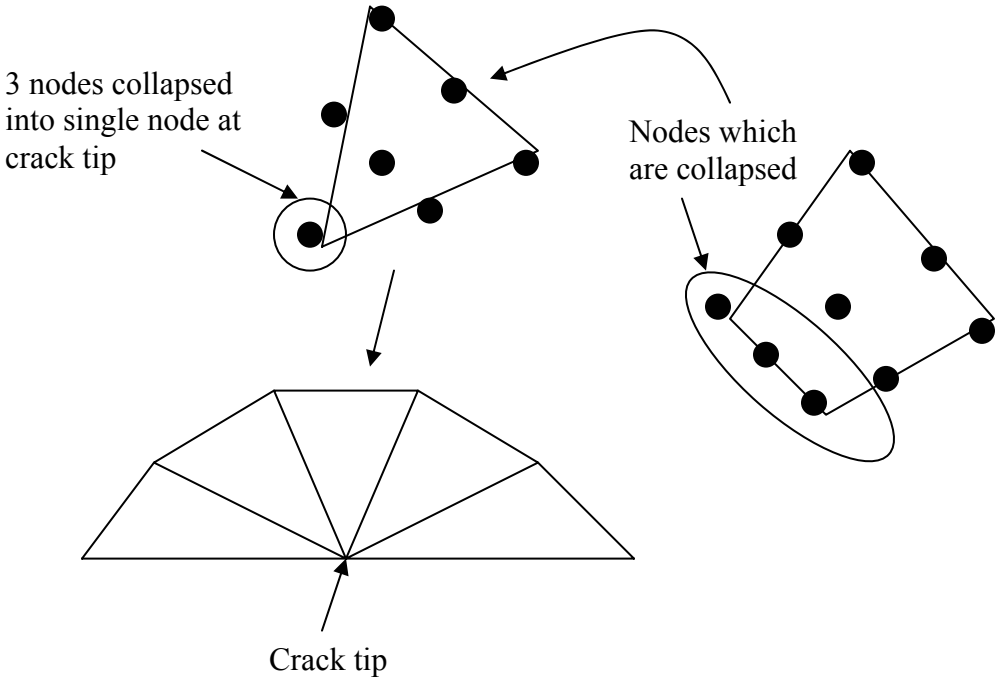

Figure 2.4: Collapsed 2-Dimensional Quadrilateral Element

$$G = \frac{K^2}{E'} \tag{2.18}$$

where

$$E' = E \text{, for plane stress} \tag{2.19}$$

and

$$E' = \frac{E}{1-\upsilon^2} \text{, for plane strain} \tag{2.20}$$

Moreover, the energy release rate can be related to total strain energy, U, as

$$G = (-1)^n \frac{1}{B}\left(\frac{dU}{da}\right) \tag{2.21}$$

where U is the strain energy stored in the body, B is the specimen thickness, and n=1 for displacement control and n=2 for load control. Given the relationship between energy release rate and the fracture mechanics parameter of stress intensity, it is possible to evaluate the parameter if one can determine the change in the potential energy of a body with crack extension. The analogous expression for nonlinear materials is given by

$$J = -\frac{d\Pi}{dA} \tag{2.22}$$

Rice [13] showed that this energy release rate is equivalent to a path independent contour integral given by

$$J = \int_{\Gamma}\left(wdy - T_i \frac{\partial u_i}{\partial x}_i \, ds\right) \tag{2.23}$$

where the strain energy density, w, is defined as follows:

$$w \equiv \int_0^{\varepsilon_{ij}} \sigma_{ij} \partial \varepsilon_{ij} \tag{2.24}$$

The components, T_i, constitute the traction vector, u_i are the displacement vector components, and ds is the differential element of the contour path Γ. The traction, T_i, is the stress normal to the contour such that

$$T_i = \sigma_{ij} n_j \tag{2.25}$$

Figure 2.5 illustrates the domain integral concept. Equating (2.18) and (2.22), we can see that for the special case of linear elastic material,

$$J = G = \frac{K^2}{E'} \tag{2.26}$$

Implementation of (2.23) into a finite element approach requires careful consideration of situations which may result in path dependence. These situations include initial strains, thermal strains and the presence of plastic deformation. In spite of these difficulties, the energy domain approach can be modified to include such capabilities as the handling of initial strains (residual stress fields), etc. These modifications allow the exploitation of the domain integral approach to determine stress intensity solutions in a broad range of situations. The details of this modification and its implementation are not presented, however, as this approach is not optimum for the problem at hand. J-contour integrals allow the evaluation of stress intensity parameters for a single crack length, with a single analysis, but require tedious detail in the construction of proper domains. This work will take the simpler approach of potential energy changes with crack extension as in equations (2.17-2.21). Specific procedures and methodologies will be detailed in Chapter 6.

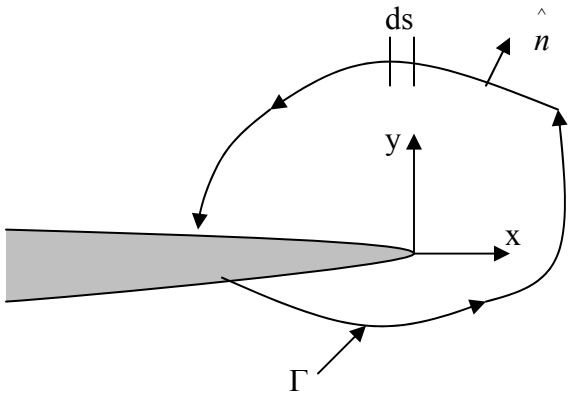

Figure 2.5: Illustration of Domain Integral Concept

2.4 Limitations of LEFM

The American Society for Testing and Materials (ASTM) standard for K_{Ic} testing [14] requires specimen size to be limited by the following for a valid K_{Ic} test.

$$a, B, (W-a) \geq 2.5\left(\frac{K_I}{\sigma_{ys}}\right)^2 \tag{2.27}$$

Here, a is crack length, B is specimen thickness and W is specimen width. The thickness requirement is meant to ensure plane strain conditions while the restriction on the in-plane dimensions ensures the crack tip behavior is linear elastic, and that K does, indeed, characterize the crack-tip conditions. The in-plane dimension requirement can be better understood by noting that a first order estimate of the plastic zone size at a crack tip is

$$r_y = \frac{1}{2\pi}\left(\frac{K_I}{\sigma_{ys}}\right)^2, \text{ plane stress} \tag{2.28}$$

and

$$r_y = \frac{1}{6\pi}\left(\frac{K_I}{\sigma_{ys}}\right)^2, \text{ plane strain} \tag{2.29}$$

Elastic stress analysis becomes increasingly inaccurate as the size of this plastic zone increases. Several researchers have derived simple corrections for mild crack tip plasticity applicable to linear elastic fracture. Irwin [15] derived a correction based on an effective crack length, $a_{eff} = a + r_y$, which, for a through crack in an infinite plate in plane stress results in

$$K_{eff} = \frac{\sigma\sqrt{\pi a}}{\sqrt{1-\frac{1}{2}\left(\frac{\sigma}{\sigma_{ys}}\right)^2}} \tag{2.30}$$

Dugdale [16] and Barenblatt [17] proposed the strip yield model, which resulted in the correction

$$K_{eff} = \sigma\sqrt{\pi a \sec\left(\frac{\pi\sigma}{2\sigma_{ys}}\right)} \tag{2.31}$$

This form for K_{eff} was later modified by Burdekin and Stone [18] to reflect more realistic values of a_{eff}. Their resulting form was

$$K_{eff} = \sigma_{ys}\sqrt{\pi a}\left[\frac{8}{\pi^2}\ln\sec\left(\frac{\pi\sigma}{2\sigma_{ys}}\right)\right]^{\frac{1}{2}} \tag{2.32}$$

Thus it is clear that while linear elastic fracture mechanics predicts a linear relationship between stress intensity factor and stress, plasticity corrections will deviate from linearity, resulting in higher effective stress intensities as the applied stress approaches yield stress. These limitations, then, demand special consideration when applying LEFM concepts. If excessive plasticity is a possibility, another parameter, which incorporates large scale plasticity, should be used.

Chapter 3

Fatigue

In this chapter, the classic stress-based and strain-based approaches to fatigue are reviewed. Fatigue crack growth is then examined in terms of power law type models. Various effects on fatigue crack growth are examined, and finally, the concepts of crack closure and overloading are presented.

3.1 Classic Approaches

The traditional approach to fatigue is based on the analysis of the average or nominal stress in an area of the structure or component being analyzed. This stress is typically adjusted in the presence of stress raisers and the resistance to this adjusted stress, under cyclic loading, determined. This is known as the stress-based approach to fatigue. A more general approach involves more detailed analysis of the local yielding which can occur at stress raisers during cyclic loading. This approach is known as strain-based.

3.1.1 Stress-Based Approach to Fatigue

The stress-based approach to fatigue typically involves the experimental determination of stress versus life (S-N) curves. A schematic S-N curve is shown in figure 3.1. Note here that S_a is the net section nominal or average stress amplitude, and must be adjusted by a stress concentration factor, k_t, for point stresses near geometric stress raisers such as holes, corners or cracks.

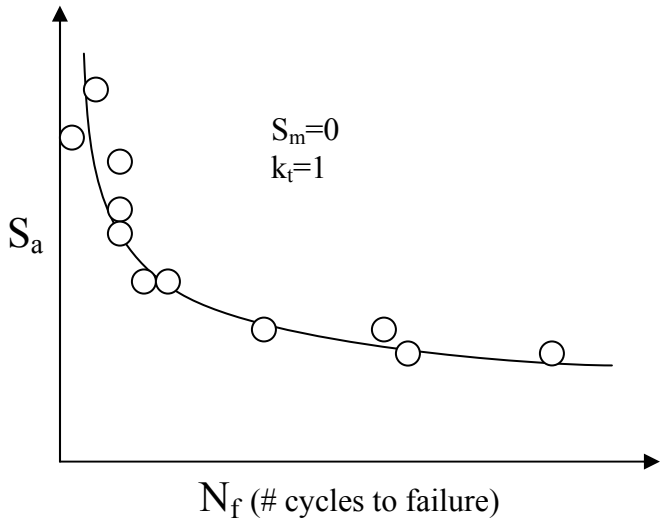

Figure 3.1: Schematic S-N Curve

Figure 3.2 illustrates the concept of the cyclic nominal stress amplitude, S_a, and the mean nominal stress, S_m. Note that typical S-N curves plot N_f, number of cycles to failure, on a log scale and stress on a linear or log scale. When a log-linear plot is used, and if the data appear to approximately fit a straight line, the data can be represented as

$$S_a = C + D\log(N_f) \tag{3.1}$$

where C and D are fitting constants. If a log-log plot is used, and the data appear to fit a straight line, then the fitted form is

$$S_a = AN_f^{\ B} \tag{3.2}$$

Dowling [19] notes that for some materials, there appears to be a stress level below which fatigue failure does not occur. This limiting stress level is typically referred to as the fatigue limit or endurance limit. For materials exhibiting this behavior, the stress level at which the endurance limit occurs is considered to be a material property. For materials which do not exhibit the behavior, arbitrary life values are typically used to assign an endurance limit. Fatigue strength, on the other hand, refers to the stress amplitude corresponding to *any* specified life. Figure 3.3 illustrates the concepts of fatigue limit and fatigue strength.

In general, the stress-based approach to fatigue is useful for longer lives (>10^4 cycles). Stress-based fatigue is most practical in situations involving low stress levels (high cycle) relative to yield stress. In the low cycle range, where yielding effects can dominate the behavior, a strain-based approach may be more appropriate. This strain-based approach to fatigue is the subject of the following section.

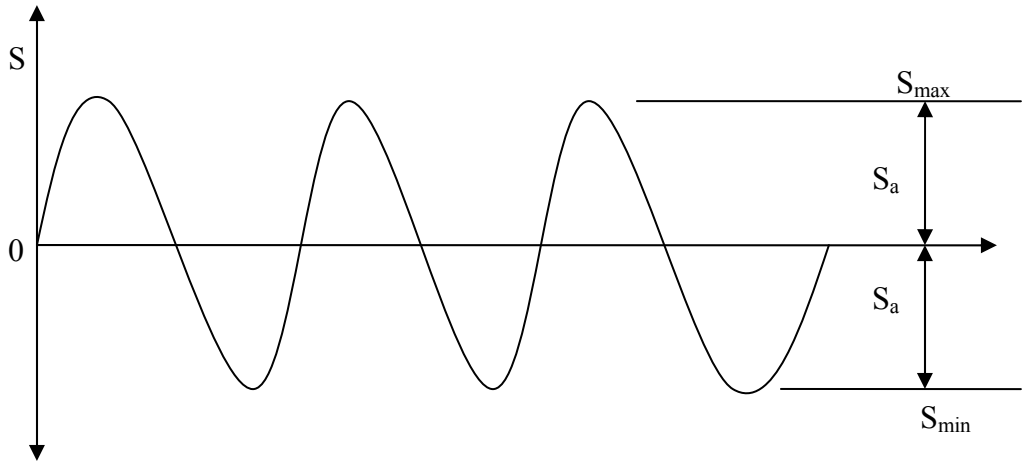

(a)

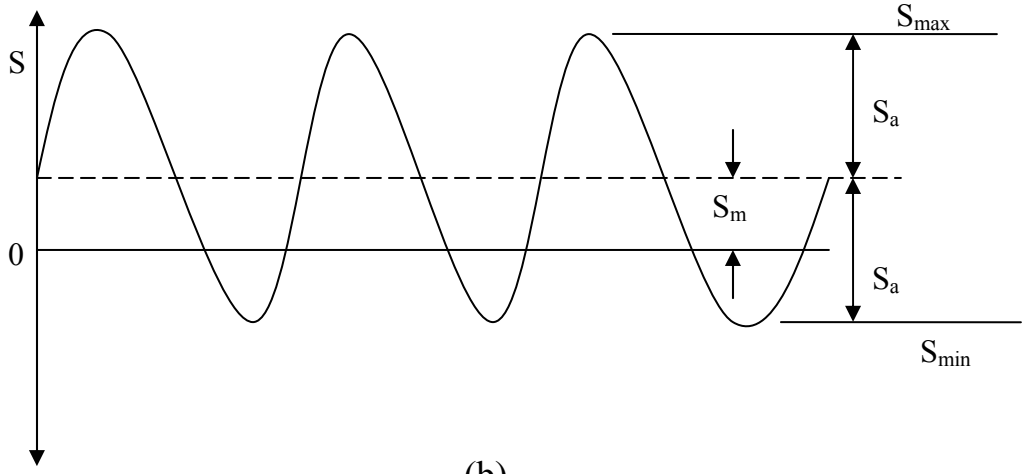

(b)

Figure 3.2: Cyclic Nominal Stress: (a) constant amplitude and zero mean stress, and (b) constant amplitude and nonzero mean stress.

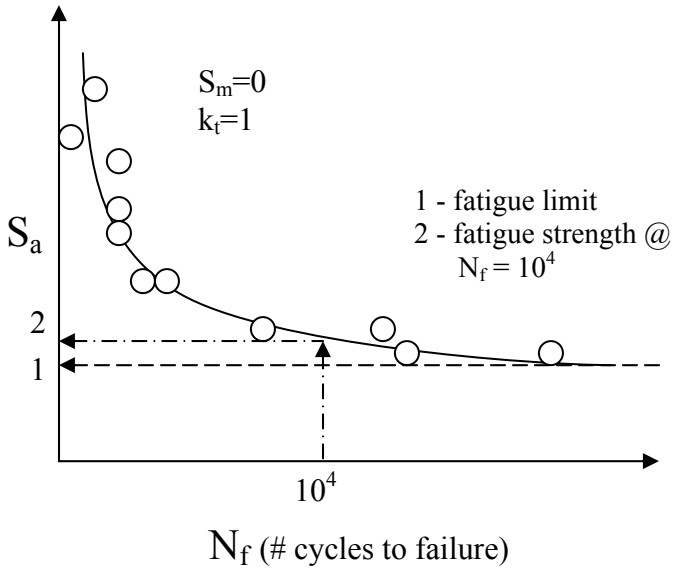

Figure 3.3: Illustration of Fatigue Limit and Fatigue Strength

3.1.2 Strain-Based Approach to Fatigue

The strain-based approach to fatigue considers localized regions of plasticity and the stresses and strains that occur in those regions. The regions of concern typically contain stress raisers or other high-stress geometric features where fatigue cracks may originate. The most distinguishing feature of a strain-based approach is the concern with a local, as opposed to a nominal, or average, stress.

Employment of a cyclic stress-strain curve is a key feature of the strain-based approach and leads directly to the development of a strain-life curve. A cyclic stress-strain curve is shown in figure 3.4. The curve is described mathematically by

$$\varepsilon_a = \varepsilon_e + \varepsilon_p = \frac{\sigma_a}{E} + \left(\frac{\sigma_a}{H'}\right)^{\frac{1}{n'}} \tag{3.3}$$

where H' and n' are curve fitting constants derived from fitting a strain hardening form of the stress-strain relationship

$$\sigma = H\varepsilon_p^n \tag{3.4}$$

and where ε_e and ε_p are the elastic and plastic strains, respectively. Equation (3.3) is known as the Ramberg-Osgood Relationship. Using this relationship, the elastic and plastic strain amplitudes can be plotted separately on a log-log scale versus the number of cycles to failure and fit to the following forms;

$$\varepsilon_e = \frac{\sigma_a}{E} = \frac{\sigma'_f}{E}(2N_f)^b \tag{3.5}$$

$$\varepsilon_p = \varepsilon'_f\left(2N_f\right)^c \tag{3.6}$$

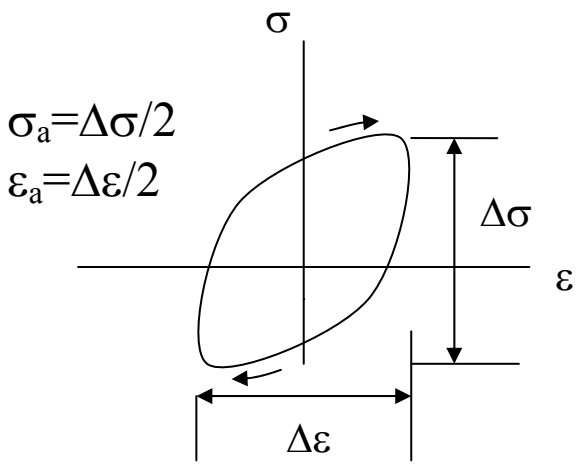

Figure 3.4: Cyclic Stress-Strain Curve (schematic)

where the fitting parameters obtained are considered material properties. This form of strain life relationship is known as the Coffin-Manson relationship. Figure 3.5 illustrates how the fitting parameters of equations (3.5) and (3.6) are obtained. In general, long lives are dominated by the first term of equation (3.3), the elastic strain. In that case, the cyclic stress-strain curve would appear thin since very little (if any) plastic deformation would be present. However, shorter lives, where significant plastic deformation is occurring, are dominated by the second term of equation (3.3), the plastic strain. At the intersection of the elastic and plastic curves of figure 3.5, a transition fatigue life, N_t, is defined. Equating equations (3.5) and (3.6) results in

$$N_t = \frac{1}{2}\left(\frac{\sigma'_f}{\varepsilon'_f E}\right)^{\frac{1}{c-b}} \tag{3.7}$$

This transition fatigue life is obviously material specific and provides a defined point for consideration of the separation of low-cycle and high-cycle fatigue. Lives near or less than the transition life may need the plasticity considerations provided by a strain-based approach, while longer lives can be safely analyzed with the simple stress-based approach. Neither approach, however, attempts to deal with the question of a pre-existing defect, nor its quantitative effect on fatigue life. To address such questions, a discussion of the fracture mechanics approach to fatigue must be opened.

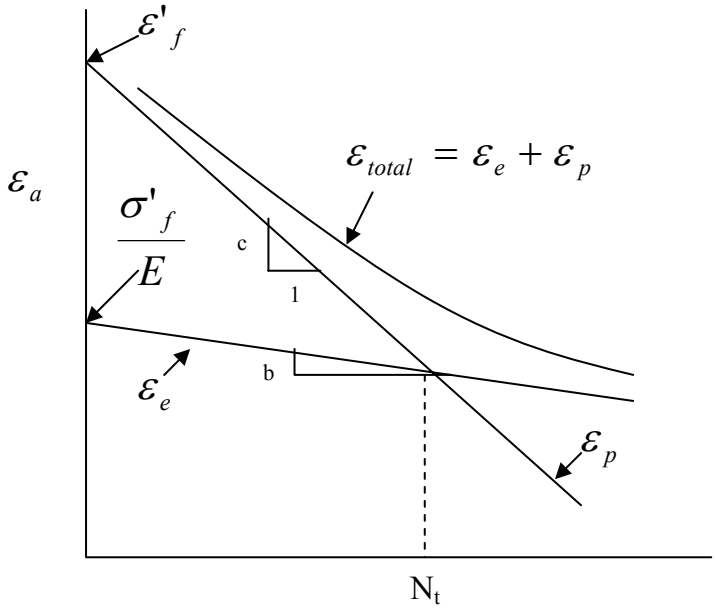

Figure 3.5: Definition of Strain-Life Parameters

3.2 Fatigue Crack Growth

Assuming a situation in which the cyclic plastic zone formed at a crack tip is sufficiently small as to remain embedded within the elastic singularity zone, such that the stress intensity factor, K, uniquely characterize the crack-tip conditions, the fatigue crack growth rate can, in general, be written as

$$\frac{da}{dN} = f\left(\Delta K, R\right) \tag{3.8}$$

where $\frac{da}{dN}$ is the crack growth per cycle,

$$\Delta K \equiv K_{\max} - K_{\min} \tag{3.9}$$

and

$$R \equiv \frac{K_{\min}}{K_{max}} \tag{3.10}$$

This simple form assumes no history effects and can be integrated to get an estimated life as follows

$$N = \int_{a_0}^{a_f} \frac{da}{f\left(\Delta K, R\right)} \tag{3.11}$$

If history effects are important, such as in overloading or non-constant load ratios, the above estimates may be in significant error, and more complicated methods may be required. In many cases, however, relationships such as equation (3.8) provide reasonable and conservative estimates for fatigue life, since effects such as those of infrequent overloading tend to lengthen fatigue life. This section details various relationships of the form of equation (3.8), beginning with the Paris Law, and discusses the factors affecting fatigue crack growth which have been

incorporated into more complicated relationships. These factors include load ratio, overloading, crack closure and the threshold stress intensity range.

3.2.1 Paris Law

Paris and Erdogan [4] proposed the power law relationship

$$\frac{da}{dN} = C\left(\Delta K\right)^m \tag{3.12}$$

where C and m are constants determined from fitting experimental data. This law applies only to the linear region of the fatigue crack growth curve (figure 1.1, region II). Their proposal initially involved an exponent of $m = 4$, but subsequent studies have shown that m can vary from 2 to 7, depending on the material. While this equation has some utility in calculating life estimates under certain conditions, it does not account for many of the important factors that can affect fatigue crack growth. These factors are discussed next.

3.2.2 Load Ratio Effects

As previously noted in equation (3.10), the load ratio, R, is the ratio of minimum stress intensity to maximum stress intensity during the cycle. In general, an increase in this ratio causes the rate of crack growth to increase. This effect is more pronounced for more brittle materials, and for more ductile materials, the effect is sometimes negligible in region II of the fatigue crack growth curve. Several researchers have proposed fatigue crack growth laws that account for the load ratio. Forman [20] proposed that

$$\frac{da}{dN} = \frac{C\Delta K^m}{(1-R)(K_c - K_{\max})} \tag{3.13}$$

represented a viable relationship for predicting behavior in regions II and III of the fatigue crack growth curve, where K_c represents the value of stress intensity factor at failure. A second relationship is based on the Walker [21] relationship relating mean stress and load ratio as

$$\Delta\overline{S} = S_{\max}(1-R)^{\gamma} \tag{3.14}$$

where $\Delta\overline{S}$ is an equivalent zero to tension ($R = 0$) stress range, and γ is an adjustable parameter. Carrying this idea over to the stress intensity factor results in

$$\Delta\overline{K} = K_{\max}(1-R)^{\gamma} \tag{3.15}$$

This relationship, after further manipulation and substitution, results in

$$\frac{da}{dN} = \frac{C_1(\Delta K)^{m_1}}{(1-R)^{m_1(1-\gamma)}} \tag{3.16}$$

where C_1 and m_1 are the appropriate constants for the $R = 0$ case. Here it is clear that the intercept, C, is a function of R, but the slope, m, is unaffected by R. In the most common analyses, however, where the primary concern is in region II of the fatigue crack growth curve, the effect of R is essentially ignored, and fatigue life calculations are based on ΔK alone. While the effect of R is sometimes negligible in certain materials for region II fatigue crack growth, the same cannot be said for region I where the growth rates are significantly lower. The following section describes the

threshold value of the stress intensity factor range, ΔK_{th}, and the effects of R-ratio on this value.

3.2.3 ΔK_{th} and Crack Closure

As shown in figure 1.1, the threshold stress intensity factor range is defined as the value of stress intensity range below which there is essentially no crack growth. Klesnil and Lukas [22] proposed a modification to the Paris equation (3.12), which took the form

$$\frac{da}{dN} = C\left(\Delta K^m - \Delta K_{th}^m\right) \tag{3.17}$$

to account for the effect of threshold on fatigue crack growth. McEvily [23] developed an equation which attempted to account for the entire fatigue crack growth curve which has the following form:

$$\frac{da}{dN} = C\left(\Delta K - \Delta K_{th}\right)^2 \left[1 + \frac{\Delta K}{K_{crit} - K_{\max}}\right] \tag{3.18}$$

One notable problem with these equations is that the threshold value typically depends on the R-ratio. Elber [24] proposed an explanation for both the fatigue threshold and the R-ratio effects. He noticed that at low loads, the fatigue specimen compliance was very close to that of an un-cracked body, while at higher loads, the compliance shifted considerably. Elber proposed that this change in stiffness was due to crack face contact, or crack closure. Figure 3.6 schematically illustrates the change in compliance attributed to crack closure. Elber further explained that crack closure reduced the effective stress intensity range, thus decreasing fatigue crack

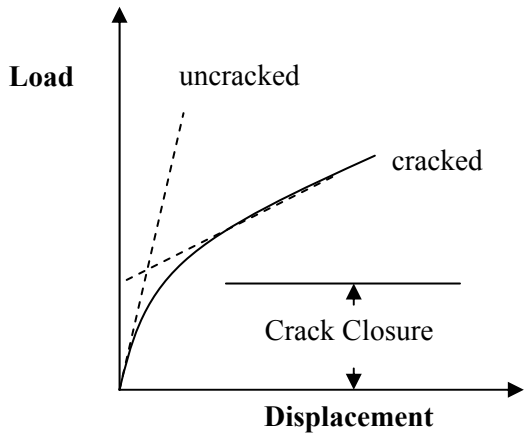

Figure 3.6: Load-Displacement Curve Illustrating Crack Closure

growth rates. To do this, he proposed the concept of K_{op}, the stress intensity below which the crack faces remain in contact. Thus the part of a stress cycle below K_{op} should not contribute to any crack growth. Elber defined the effective stress intensity range as

$$\Delta K_{eff} = K_{\max} - K_{op} \tag{3.19}$$

This value of ΔK_{eff} can then be used in the Paris equation (3.12) to give

$$\frac{da}{dN} = C\Delta K_{eff}^{m} \tag{3.20}$$

Figure 3.7 illustrates the concept of K_{op} and ΔK_{eff}.

Later research has shown that crack closure does indeed occur during fatigue crack growth. Suresh and Ritchie [25] identified multiple modes of crack closure, including closure produced by plastic stretching of the crack faces. The discoveries of crack closure have thus provided a physical model to explain the phenomenon of threshold stress intensity range.

The model developed by Elber provides an explanation of threshold stress intensity, but leaves the question of its dependence on R-ratio open. With the following relationship defined,

$$U \equiv \frac{\Delta K_{eff}}{\Delta K} \tag{3.21}$$

various researchers [26-28] have shown that empirical relationships of the form

$$U = a + bR \tag{3.22}$$

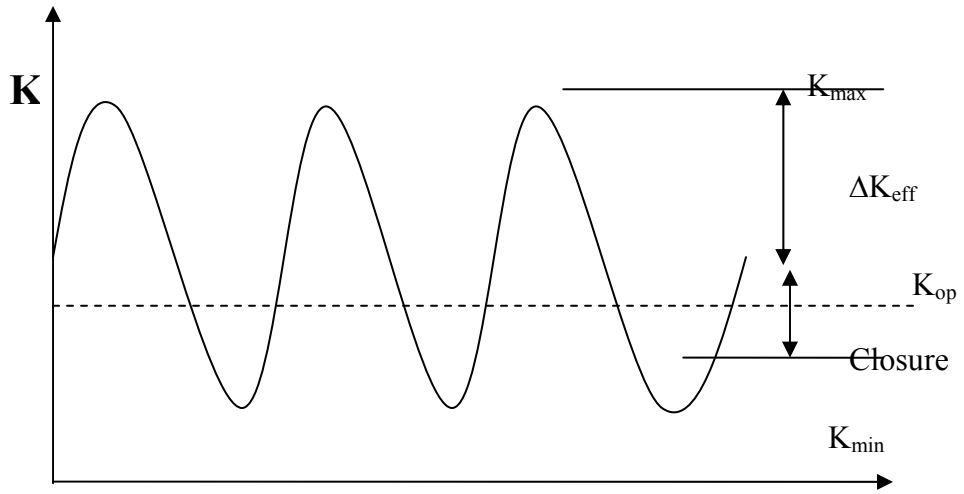

Figure 3.7: Definition of Effective Stress Intensity Factor Range

where a and b are fitting constants, can be used to describe the dependence of effective stress intensity on R-ratio. Shih [29] has since disputed this simplified approach and has claimed a dependence of U on other factors, namely $K_{\max}$. Apparently, no single relationship developed thus far is sufficient for describing the phenomenon of crack closure in all three regions of the fatigue crack growth curve.

3.2.4 Overload Effects

Consider a fatigue loading history where a constant amplitude series is interrupted by a single tensile overload, followed by a return to the previous constant amplitude loading. In this situation, it has been well documented that a retardation effect is observed which results in a decreased fatigue crack growth rate. The overloading results in compressive residual stresses in the region surrounding the crack tip, which account for the decreased crack growth rate. Once the crack grows through the overload plastic zone, the crack growth rate returns to its previous value.

Wheeler [30] proposed a model which considers the size of the overload plastic zone in relation to the size of the current plastic zone. The overload plastic zone is given by

$$r_y = \frac{1}{\alpha\pi}\left(\frac{K_0}{\sigma_{ys}}\right)^2 \tag{3.23}$$

where K_0 is the stress intensity at the peak of the overload cycle, and $\alpha = 2$ for plane stress and $\alpha = 6$ for plane strain. The current plastic zone size, corresponding to $K_{\max}$, is given by

$$r_C = \frac{1}{\alpha\pi}\left(\frac{K_{\max}}{\sigma_{ys}}\right)^2 \tag{3.24}$$

In his model, Wheeler assumed that the retardation effect of the overload plastic zone lasts as long as the current plastic zone is contained within the overload zone boundaries. As soon as the current plastic zone touches the boundary of the overload plastic zone, Wheeler suggested that the retardation effect stops. Wheeler also defined a retardation factor, ϕ_R, which is a function of the two plastic zone sizes, and the total crack increment since overload. The retardation factor he proposed also employed a fitting parameter which requires experimental determination for each separate material and stress spectrum, thus limiting its practical use.

Other models, which attempt to account for the retardation effect of an overload, deal primarily with the plastic wake left behind the growing crack. This plastic wake is a function of load history and as such, provides a method of including crack closure effects. The effects of the plastic wake on crack closure have been documented by Suresh and Ritchie [25], and these effects result in a lower effective stress intensity factor range, ΔK_{eff}, as discussed earlier. Newman [31] developed a crack closure model based on such plastic wake effects which can be used to make predictions of fatigue life under variable amplitude loading.

While the substance of the current research is not necessarily concerned with overload effects, per se, it is profoundly dependent on the questions surrounding general residual stresses and their effects on fatigue crack growth. As such, the inclusion of this brief discussion of overload

effects has given some insight into current thoughts directly related to the more general problem of residual stress effects.

Chapter 4

Residual Stress Overview

The formation of residual stresses can, in general, be classified into two types: mechanical and thermal or transformational. In the practical sense, a growing crack does not discern the type of residual stress, for the end result on the growing crack is identical, regardless of type. From this viewpoint, a residual stress can be described quantitatively as resulting from an incompatible strain field. This quantitative approach is discussed further in a later chapter pertaining to the current research. A more qualitative description is, however, possible considering the physical phenomena which produce residual stress fields. An introduction to these phenomena is the purpose of this chapter.

4.1 Mechanically Induced Residual Stresses

Consider a beam loaded in bending as shown in figure 4.1(a). The nonlinear distribution of stress represents a yielding condition where the stresses at the upper and lower surfaces have both exceeded the yield strength of the material, one in tension, the other in compression. Upon unloading, the material at a distance from either surface, not having plastically deformed, attempts to recover its original, zero strain, condition, but is resisted by the yielded material closer to the surface. The result on the tension side of the beam, upon self-equilibration of internal stresses, is a compressive residual stress field near the surface, which transitions to a tensile residual stress at some distance away from the surface. The result on the compressive side of

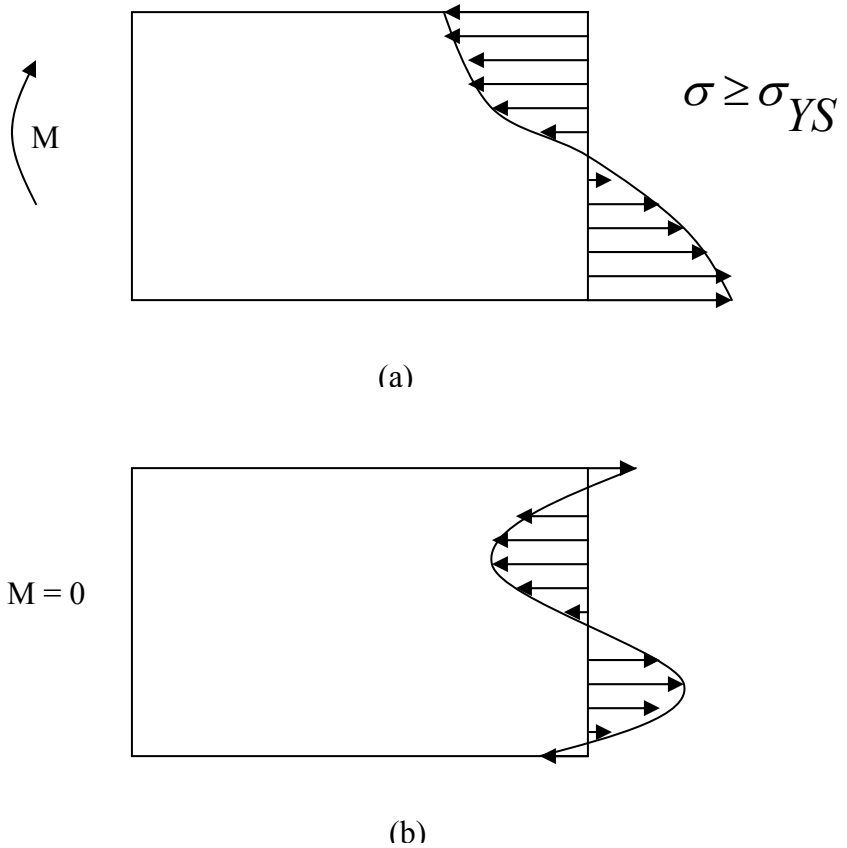

Figure 4.1: Plastic Loading of a Beam: (a) beyond yield, and then (b) unloading

the beam is mirrored along the plane perpendicular to the stress as in figure 4.1(b). While this example is a gross simplification of what can be a somewhat complicated process, it serves the purpose of illustrating the general concept of mechanically induced residual stresses.

4.2 Phase Transformation-Induced Residual Stress

Just as mechanical loading can cause a yielding condition within a structure or component, so too can a thermal load. Consider, for example, a thin steel rod, under an intense thermal load such that only the layers closest to the surface are initially heated. As the surface of the steel rod heats up it undergoes a phase transformation from the body-centered cubic ferrite to face-centered cubic austenite, and a contraction in the material takes place, which is resisted by the ferritic inner layers of material. At this point, the surface layer is in tension, and the center in compression. Due to the lower yield strength of the austenitic phase, and due to its relatively small cross-sectional area, the surface can plastically deform under the tensile stress, thus temporarily relieving all internal stress. When the thermal load is removed, and the surface begins to cool, a phase transformation from austenite to other products begins and the surface attempts to expand, but is restrained by the ferritic center. This leaves the surface layers in a state of compressive residual stress. This sequence of events is illustrated schematically in figure 4.2. Again, the example is a simplified one for purposes of illustrating fundamental concepts. In reality, the situation involving residual stress formation due to phase transformations and thermal

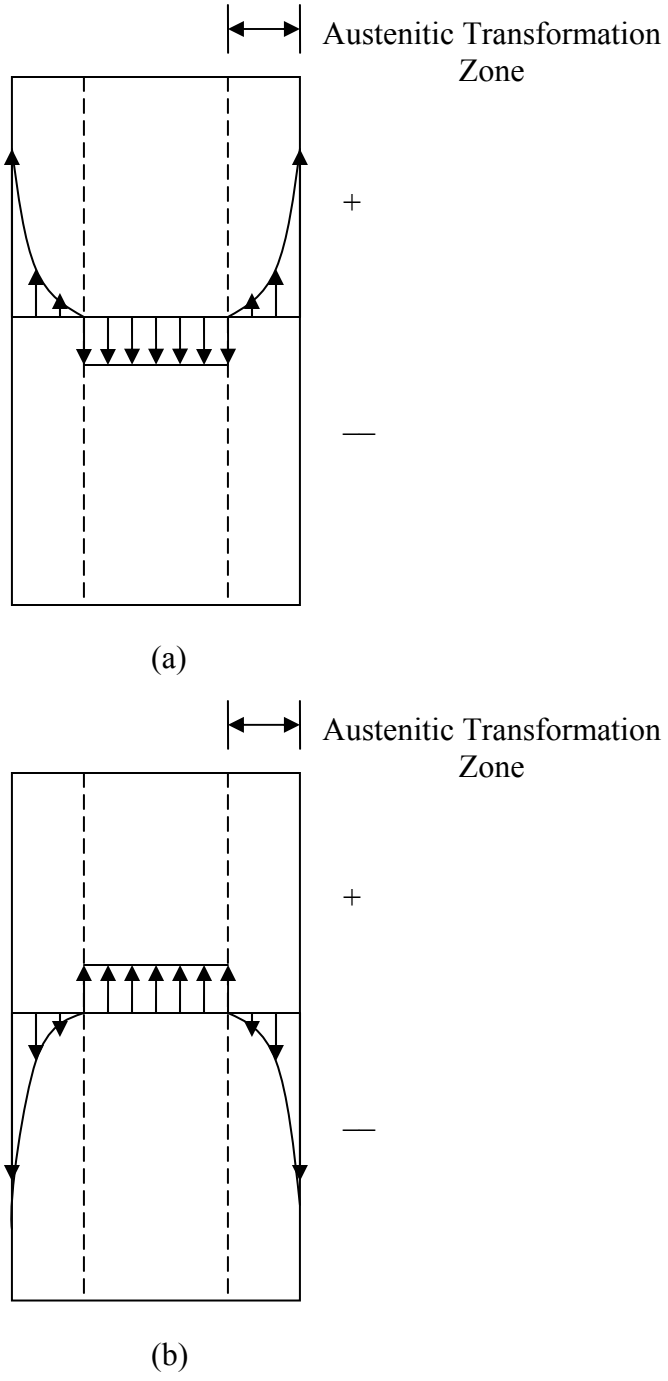

Figure 4.2: Transformation-Induced Residual Stress Distribution: (a) after surface thermal load produces austenitic phase transformation but before plastic deformation takes place, and (b) after subsequent cooling

loading can be extremely complex. Volumetric expansion and contraction of the different possible austenitic decomposition products is complicated by normal thermal expansion as well as the uncertainty of which products will indeed form via the transformation. The actual composition of the decomposed austenite depends largely on the cooling rate from the austenitic temperature range, which obviously varies through the cross section. Thus it is quite possible to have a range of microstructures form from a single thermal event, each having a different magnitude of expansion or contraction. As one can easily see in a case such as this, accurate prediction of the actual residual stress distribution is near impossible. In most practical cases, predictions of residual stress distributions are based on empirical data derived from destructive methods such as cutting or drilling the samples and recording variable data from attached strain gages. For the current research, certain simplified residual stress distributions are documented and their descriptions are given in terms of the physical situation from which they may originate.

4.3 Measurement of Residual Stresses

Residual stress measurement techniques can be broken down into two general categories, quantitative methods and qualitative methods. The qualitative methods, such as photo stress coatings, while providing valuable information under certain circumstances, are becoming secondary tools used only in rough screening processes. Walker [32] suggests that strain gages and diffraction techniques, which comprise the majority of the more advanced quantitative methods have, in the last several years, become the

most widely preferred analysis tools in residual stress quantification. For this reason, discussion of residual stress measurement methods will be limited to these, more common, quantitative methods.

4.3.1 Strain Gage Methods

Probably the most common of all the quantitative methods of residual stress measurement involves the use of strain gages to measure changes in strain upon destruction of the body's equilibrium state. The equilibrium state is changed by removing material from the structure or component of interest. During this removal of material, the strain tensor at any given point in the body will change as equilibrium is re-established. These changes in strain are typically measured by strain rosettes, strategically mounted on the body, which take three linearly independent strain measures (for plane strain). Figures 4.3 and 4.4 illustrate the concept of the strain gage rosette. The transformation of strains with respect to {X,Y,Z} coordinates is performed with the following:

$$\begin{aligned}
\varepsilon_{x'} &= \frac{(\varepsilon_x + \varepsilon_y)}{2} + \frac{(\varepsilon_x - \varepsilon_y)}{2}\cos 2\theta + \varepsilon_{xy}\sin 2\theta \\
\varepsilon_{y'} &= \frac{(\varepsilon_x + \varepsilon_y)}{2} - \frac{(\varepsilon_x - \varepsilon_y)}{2}\cos 2\theta - \varepsilon_{xy}\sin 2\theta \\
\varepsilon_{x'y'} &= -\frac{\varepsilon_x - \varepsilon_y}{2}\sin 2\theta + \varepsilon_{xy}\cos 2\theta
\end{aligned} \tag{4.1}$$

Substitution of α, β, γ, ε_a, ε_b, and ε_c into equations (4.1), results in a system of three equations with three unknowns. The solution for these three unknowns represents the three strain components of plane strain.

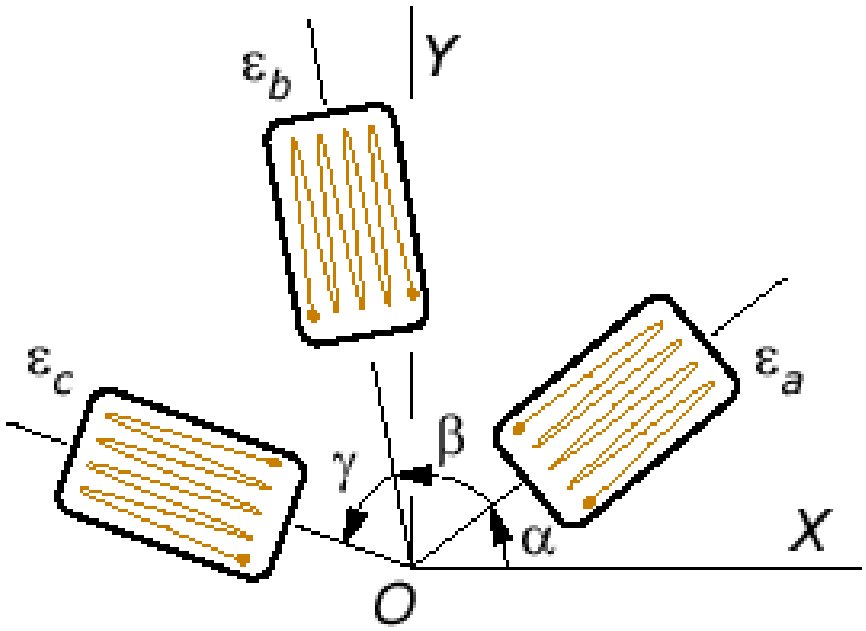

Figure 4.3: Example of a Strain Rosette Configuration

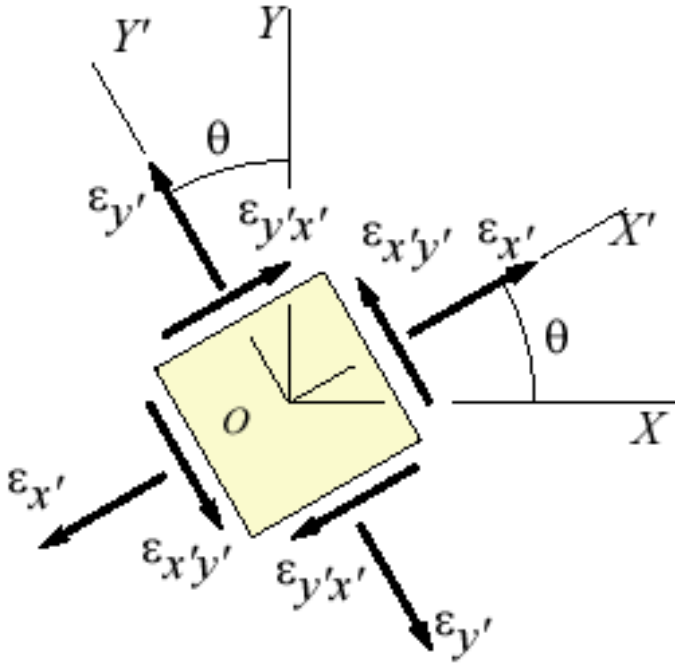

Figure 4.4: Coordinate Axes Definitions for Strain Transformation

Many configurations of strain gages are possible, and many alternate methods of destructive evaluation involving measurement of strain changes have been developed over the years. Hill [33] provides a detailed analysis of the more common strain gage methods.

4.3.2 Diffraction Methods

Two common diffraction methods for determination of residual stresses are prevalent in modern research. The first, used predominantly for measuring surface residual stresses (8-20μm below surface), is the X-ray diffraction method. The second, used to measure residual stresses at much greater depths (up to 152 mm in aluminum, 38 mm in steel), is neutron diffraction. Both methods are based on the physical principles of the interaction of electromagnetic radiation and matter. The fundamental mathematical description of diffraction is given by Bragg's Law,

$$n\lambda = 2d\sin\theta \tag{4.2}$$

where n is an integral multiple of the wavelength, λ, d is the distance between adjacent planes of atoms in the material being examined, and θ is the angle of incident radiation. Bragg's Law is easily derived by referring to figure 4.5. The two incident and refracted beams, while having the same incident and refracted angles respectively, travel different distances. The lower beam travels an additional distance of $AB + BC$. Since $AB = BC$, and since the difference in distance traveled between the two beams must be an integer multiple (n) of the characteristic wavelength, λ, it is clear that $n\lambda = 2AB$. Noting the geometry of the incident angle and its relationship to the distance, AB, reveals the complete form of Bragg's Law. To

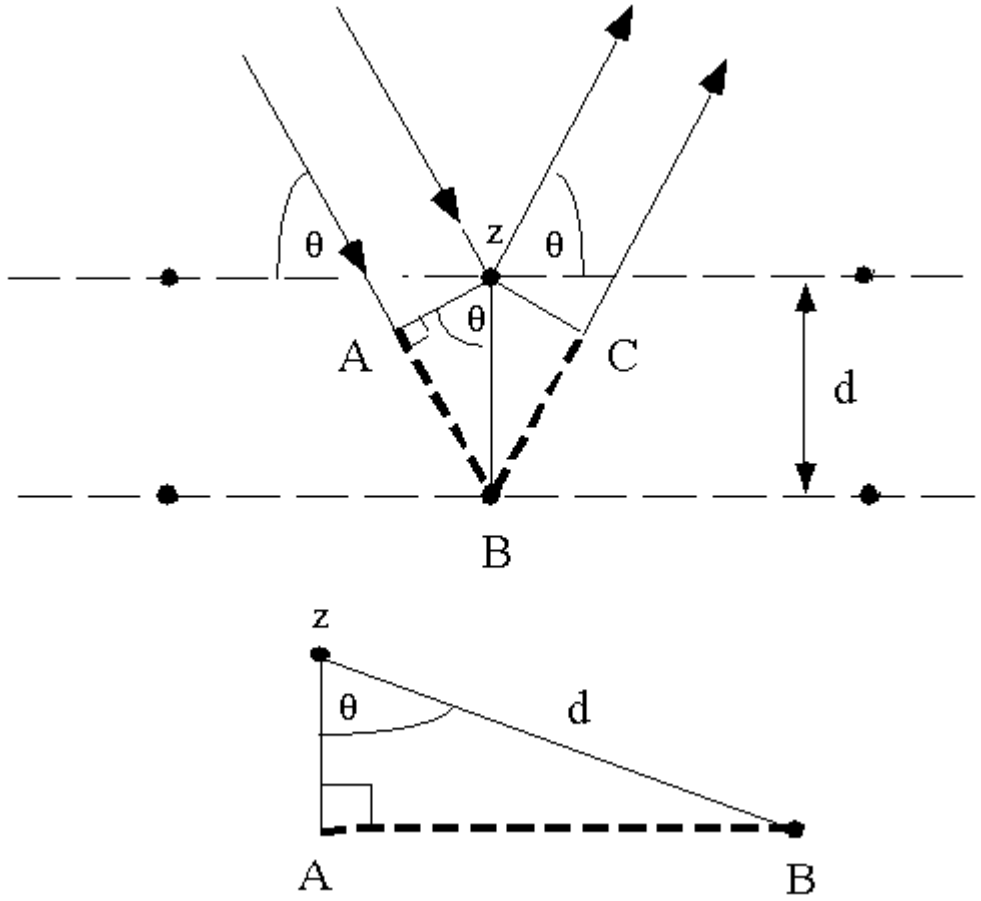

Figure 4.5: Derivation of Bragg's Law

understand how an eigenstrain, or residual strain, would affect such a relationship, one need only realize that these residual strains will change the distance between adjacent layers of atoms, and thus shift the diffraction peaks away from their characteristic θ-values.

Chapter 5

Previous Research

This chapter consists of a literature review concerning two key areas specifically related to the current research. First, the critical question of modeling residual stress in a finite element environment is addressed. The concept of eigenstrain modeling is introduced as a promising method for simulating residual stress fields in a finite element model. Second, the effects of residual stress on fatigue crack growth are reviewed including the redistribution of residual stress with crack growth, and weight function methods for approximating residual stress effects on stress intensity parameters.

5.1 Finite Element Modeling of Residual Stresses

Several commonly accepted methods exist for the introduction of residual stresses into a finite element model. The more straight forward method of simulated mechanical loading provides a means of introducing a plastic deformation within a model, which, when unloaded, results in a residual stress field. Figure 4.1 provided an illustration of the basic concept of mechanically induced residual stress. Pavier et al. [34] used such a method to introduce residual stresses into aluminum sheet material through simulation of a cold-working procedure. In his model, a rivet was pulled through an aluminum sheet in such a way as to force a radial expansion of the hole edge, followed by a contraction. While this method can be fairly straight forward, it does present some difficulty in the sense that it is extremely difficult to know, with reasonable accuracy, the residual stress

distribution one will obtain given a specified mechanical overload on a given structure. A second difficulty arises from the computational effort required when doing elastic-plastic analyses. For example, if the analyst is merely interested in a linear elastic fracture parameter of a given geometry with a given residual stress field, he/she may first be required to execute repeated elastic-plastic analyses on the model, each of which require many iterations due to the nonlinearity involved, to introduce the required residual stress.

An alternative method for introducing residual stresses into a finite element model is through imposition of proper initial conditions. O'Dowd et al. [35] illustrated how initial stresses could be imposed on a finite element model as a non-unique initial condition. The non-uniqueness arises from the fact that a given stress distribution can result from a number of different loading histories. O'Dowd also pointed out that the introduction of an initial stress field is not always a straight forward method in practice. The reason for this difficulty is that imposed initial stresses are self-equilibrated across the entire model in the first load step of an analysis, usually resulting in a stress distribution that differs significantly from the desired one. Despite these difficulties, however, the initial stress method can be used with iterative methods to properly define an initial stress distribution.

Matos and Dodds [36] approached the problem of modeling residual stresses with what Mura [37] termed an eigenstrain and what Ueda [38] referred to as an inherent strain approach. Eigenstrains refer to incompatible strain fields, denoted ε_{ij}^{*}. The incompatibility is described by the six strain compatibility equations in Cartesian coordinates as

$$R_{pq} = e_{pkl} e_{qij} \varepsilon^{*}_{ij,kl} \tag{5.1}$$

where repeated indices imply summation, the commas denote partial differentiation and e_{pkl} denotes the third order alternating tensor, also termed by Malvern [39] as the permutation symbol. When R_{pq} vanishes, no residual stress is required to maintain compatibility. The total compatible strain tensor can be written as

$$\varepsilon_{ij} = \varepsilon^{e}_{ij} + \varepsilon^{*}_{ij} \tag{5.2}$$

where ε^{e}_{ij} denotes the elastic strain tensor required to remove the incompatibility caused by the eigenstrain tensor, and from applied loading. The linear elastic stresses, therefore, must be given by

$$\sigma_{ij} = D_{ijkl}(\varepsilon_{kl} - \varepsilon^{*}_{kl}) \tag{5.3}$$

Since the elastic stress is proportional to the difference between the total strain and the eigenstrain tensors, it is possible to model the eigenstrains simply as thermal strains. In general, however, residual stress fields are highly anisotropic, and as such, require a spatial distribution of anisotropic thermal expansion coefficients for proper modeling. Hill and Nelson [40] proposed a simple method whereby a unit temperature increase is imposed on the finite element model and a spatial distribution of anisotropic thermal expansion coefficients, a_{ij}, is defined such that $a_{ij} = \varepsilon_{ij}$ at each material point within the domain. This approach has been exploited by Matos and Dodds [36] as a convenient method of modeling residual stresses. While the method provides a convenient approach to the introduction of residual stress into a finite element model, its implementation is usually not straight

forward. The difficulties inherent in this approach are discussed in Chapter 6, which deals with the specifics of this research.

5.2 Residual Stress and Fatigue Crack Growth

Fatigue crack growth in the presence of a residual stress field has been studied both experimentally and analytically for several decades. Recent research has focused on the empirically-based characterizations of material-specific fatigue crack growth behavior, and on predictive analytical models. The former, having had reasonable success, dominates the available literature on the subject, while the later has been somewhat limited to weight function type approaches.

Galatolo and Lanciotti [41] conducted fatigue crack growth tests on plasma welded 2219-T851 aluminum alloy compact tension specimens and compared the results with center cracked tension specimens with the residual stress distribution shown in figure 5.1. Their results indicated that the presence of the tensile residual stress in the area of the initial crack increased the fatigue crack growth rate over that observed in the residual stress free compact tension specimen. Galatolo and Lanciotti also recorded the stress near the crack tip as a function of crack length and the actual stress ratio, R, for each crack length. This information is shown in figure 5.2. It is clear from comparison of figures 5.1 and 5.2 that the residual stress is redistributing away from the crack tip in such a way as to create tensile residual stresses in areas where they previously did not exist. By taking into account the load ratio via the Walker equation (3.16), a reasonable agreement was reached between the fatigue crack growth rates for the two

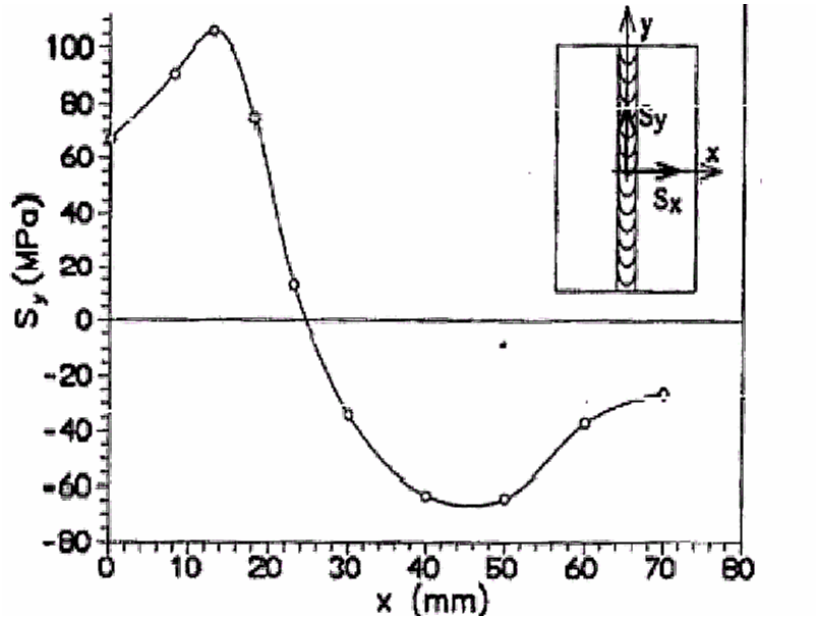

Figure 5.1: Residual Stress Distribution Obtained by Galatolo [39]

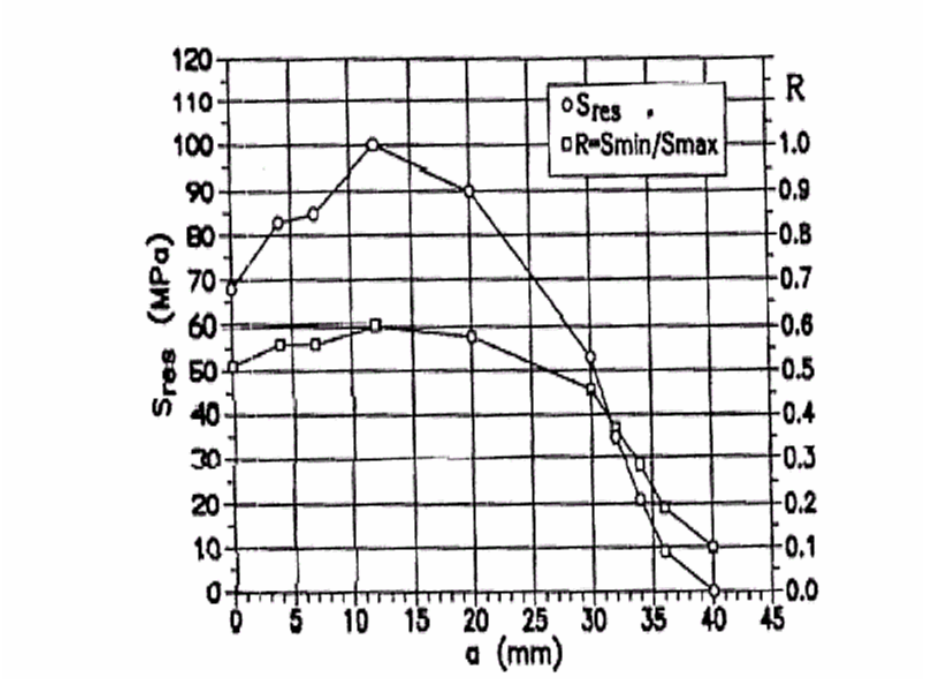

Figure 5.2: Residual Stress and Stress Ratio [39]

specimen types. Fitzpatrick and Edwards [42] witnessed these same redistribution effects on quenched plates. Their results indicated that the residual stress redistribution was enough to result in significant error in the life estimate if a weight function approach was used. Some researchers [43-45, 54] have simply ignored this redistribution on the assumption that weight function calculations, which are based on the original residual stress distribution, are sufficient. Their approach has been to consider an effective stress intensity factor defined by

$$K_{eff} = K_{app} + K_{res} \tag{5.4}$$

where K_{app} is the stress intensity due to the applied loading and K_{res} is the stress intensity due to the residual stress field. In this case, the fatigue crack growth rate is given by

$$\frac{da}{dN} = f(\Delta K_{eff}) \tag{5.5}$$

Thus the remaining requirement is an appropriate expression for K_{res}. The weight function approach provides a method for calculating the stress intensity factor for any loading, provided the weight function, which depends only upon the geometry of the body, is known. Assuming the weight function is known, or can be determined, the stress intensity can be calculated as

$$K_{res} = \int_{\Gamma_c} \sigma_{res}(x) h(x,a) dx \tag{5.6}$$

where $\sigma_{res}(x)$ is the initial residual stress distribution, $h(x,a)$ is the weight function for the specific geometry of interest, and Γ_c is the perimeter of the crack.

Other researchers have considered the effects of the redistributing stress to be of prime importance. Lee et al. [46], performed redistribution experiments on welded mild steel plates. The plates were progressively cut and the change in residual stress measured by attached strain gages. The distribution of the residual stress was based on one proposed by Masubuchi and Martin [47], which has the form

$$\sigma_r(x) = \sigma_0 \left[1 - \left(\frac{x}{b} \right)^2 \right] \exp^{\left(\frac{x}{\sqrt{2}b} \right)^2} \tag{5.7}$$

where b is the half-width of the tensile region. Figure 5.3 shows the results of this redistribution study. From the figure it is evident that stress redistribution can create tensile residual stresses in areas of the specimen where compressive residual stresses had existed initially. This could possibly result in non-conservative estimates of fatigue life if redistribution effects are not considered.

Attempts have also been made at complete analytical methods for calculating the redistributed residual stress. Fukuda [48] proposed computer algebra methods to handle the difficult integrations involved in his model of redistributing residual stress. He proposed that the residual stress after redistribution was given by

$$\sigma_{res}^{R}(a < x \le W) = \sigma_{res}^{i}\left(a < x \le W\right) + \int_0^a \sigma_{res}^{i}(\xi)\phi(a,\xi,x)d\xi \tag{5.8}$$

where a=crack length, W=specimen width, σ_{res}^{i} = initial residual stress, σ_{res}^{R} = redistributed residual stress, ϕ is the function representing the stress at $x(z < x \le W)$ when a unit load is placed at $\xi(0 \le \xi \le a)$. Although ϕ

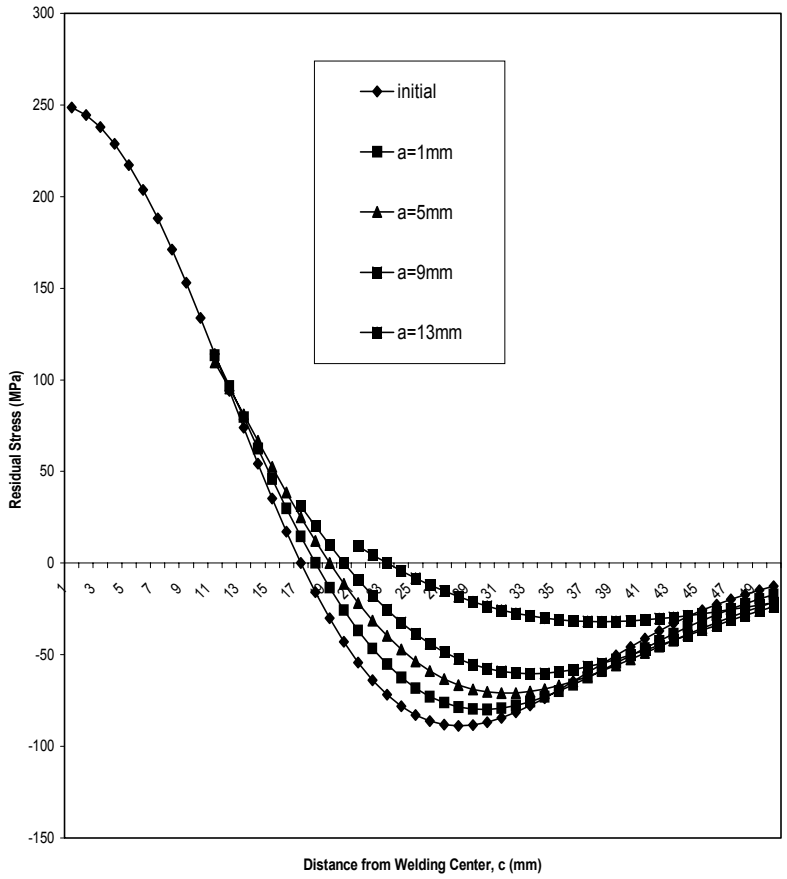

Figure 5.3: Redistribution of Residual Stress with Crack Propagation [46]

is, in practice, sometimes very difficult to obtain for finite bodies, it can be approximated with simple corrections to known solutions of infinite body problems. Fukuda's results indicated that for a freely redistributing residual stress (i.e., no constraints), this method may be quite useful, and indeed his results were in good agreement with experimental data.

Chapter 6

Research Detail

In this chapter, the details of an original research effort are outlined. A concise problem statement is first given, explaining the interesting and unique problem at hand. Methods and tools used in the research are then explained, and include finite element modeling methods, regression analysis and programming.

6.1 Problem Statement

The interaction of a growing fatigue crack with a residual stress field is not a well understood phenomenon. This lack of understanding has sometimes lead to confusing and possibly inaccurate and/or non-conservative methods being employed in fatigue life prediction problems where residual stresses are present. Redistribution of residual stress is known to occur as a result of this interaction, but its effects on the stress intensity factor, K, have yet to be quantified. Moreover, a direct comparison of K calculated via the appropriate weight function (which assumes no stress redistribution) with that of a calculation which includes redistribution sheds light on the nature of the error inherent in the weight function method. Calculations of K which include the effects of redistributing stress are considered an improvement over existing methods. *Development of a physical model and corresponding quantitative methodology for determination of residual stress effects, including that of residual stress redistribution, on fatigue life are the primary objectives of this research.*

6.2 Methods and Tools

The methods and tools used in this research are, for the most part, well established and widely used in solid mechanics and other scientific research. Classic finite element methods are employed as the main analysis tool, with the detail of its use being outlined in following sections. Standard regression analysis is also used as needed to provide functional relationships between variables. Other standard analysis methods, such as numerical integration and/or common programming tasks involving C, C++, Matlab [49] and Mathematica [50] have also been utilized as required.

6.2.1 Finite Element Analysis

The finite element code used in this research is called Warp3D [51]. Warp3D is a research code that was specifically developed for solving large-scale, three-dimensional problems with static or dynamic loading. While this code contains many attractive features, its use for this research is warranted by the following:

- Facilities to model crack growth including node release algorithms
- Ability to implement element-specific and/or anisotropic thermal expansion coefficients
- Compatibility with Patran neutral geometry files
- Intuitive command structure
- PC compatibility

6.2.1.1 Eigenstrain Implementation

The concept of eigenstrain was presented in Chapter 5 as an incompatible strain component. In this section, the practical implementation of this concept into a finite element model is explained. As noted in Chapter 5,

defining a spatial distribution of anisotropic thermal expansion coefficients and imposing a unit temperature increase on the model will result in a self-equilibrating internal stress which can be considered a residual stress. While the concept is certainly simple, the implementation can be quite cumbersome, and sometimes unpredictable. Consider the two connected elements depicted in figure 6.1. Let each element have unit length sides and be of the same material with elastic modulus, E. At the interface of the two elements, for example point 1, the strain field must be continuous and therefore the following holds:

$$\delta_e = \delta_1 + \frac{\sigma_{21}}{E} = \delta_2 + \frac{\sigma_{12}}{E} \tag{6.1}$$

where δ_e is the equilibrium displacement of point 1, δ_1 and δ_2 are the displacements which the elements would undergo if unconstrained, σ_{21} is the stress created by element 2 on element 1, and similarly for σ_{12}. Since the forces exerted by these two elements upon each other are equal and opposite, the following holds;

$$\delta_1 - \delta_2 = \frac{2\sigma_{12}}{E} \tag{6.2}$$

Solving equation (6.2) for $\frac{\sigma_{12}}{E}$ and substituting into (6.1) gives

$$\delta_e = \delta_2 + \frac{1}{2}\left(\delta_1 - \delta_2\right) \tag{6.3}$$

If the elements have sides of unit length, a unit temperature increase will result in an unconstrained expansion equal to α_n, the thermal expansion coefficient for element n. We see then that

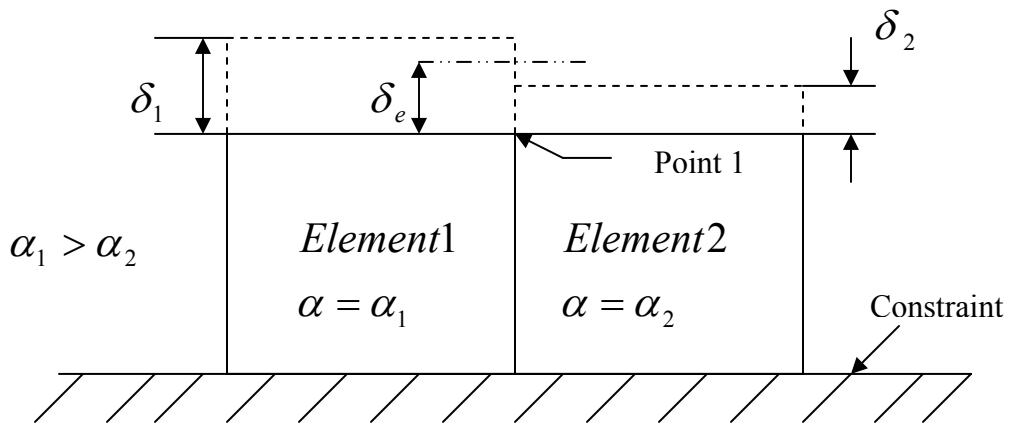

Figure 6.1: Elements with Different Thermal Expansion Coefficients Causing Mutual Residual Stress

$$\delta_e = \alpha_2 + \frac{1}{2}(\alpha_1 - \alpha_2) = \frac{1}{2}(\alpha_1 + \alpha_2) \tag{6.4}$$

which merely states that the equilibrium displacement of point 1 will be equal to the average of the thermal expansion coefficients of the two elements. From figure 6.1 it is also clear that element 1, being restrained from expanding to its full unconstrained equilibrium length, is under a compressive stress, while element 2 is under a tensile stress. Although the matter may seem trivial in the limiting case of two elements, it quickly becomes an onerous task to add elements and/or dimensions to the problem. Moreover, the possible anisotropy of the thermal expansion coefficients can make it extremely difficult to have intuition on the possible distribution of stresses, given a multi-dimensional model.

For these reasons, the modeling of residual stresses via eigenstrain implementation is most easily accomplished through trial and error. Furthermore, since the purpose of this research is to understand the effects of residual stress and its redistribution on the stress intensity parameter, K, the initial distribution of residual stress is not a critical matter. It is stated here with the aforementioned justification that the residual stress distributions to be modeled are for methodological illustration purposes only, but are modeled to be as close an approximation to real residual stress patterns as is possible within the constraints of time and of knowledge of the actual distribution.

6.2.1.2 Crack Growth Procedure

The method of crack growth simulation used in this research is known as node release. Node release involves incremental crack extension along a

symmetry plane by removal of nodal displacement constraint. When a node is released from its displacement constraint, the reaction force previously acting at the node vanishes. The release of the displacement constraint at a node affects the equilibrium state in the element containing the node, and thereby affects the equilibrium state of surrounding elements. As was shown in the previous section, adjacent elements with differing thermal expansion coefficients have a mutual impact, resulting in self-equilibrating residual stresses. If, therefore, a nodal displacement constraint is removed from one of these elements, thus affecting the equilibrium state by removing that particular nodal reaction force, the equilibrium displacement, δ_e, will change. The changing of equilibrium displacement results in a change in the residual stresses present within the two elements. This effect, known as residual stress redistribution, is one of the main effects investigated in this research.

6.2.1.3 Model Calibration

Calibration of the finite element model consists of refining the mesh until the change in potential energy with crack extension closely approximates a known solution for stress intensity factor, K. Since the change in potential energy with crack extension is approximated as an average change over a finite crack extension, a reasonably fine mesh is required to obtain accurate results. This mesh, however, is much coarser than what would be required for crack tip stress analysis.

6.2.1.4 The FE Model and Analysis

As previously mentioned, the finite element modeling and analysis was carried out using the Warp3d research code. The geometry model consists of a simple SENT specimen geometry, modeled with a symmetry plane (the crack plane), and with uniform eight (8) node isoparametric brick elements over the entire model volume. The model consists of a total of 5043 nodes and 3200 elements. Figure 6.2 illustrates the integration points of the eight-node elements, and table 6.1 provides the coordinates of these points, in terms of parametric coordinates. Standard 2x2x2 Gauss quadrature is used in evaluating these eight-node isoparametric elements. For all analyses reported in this research, stress and/or strain values are taken at the parametric center points of the elements, or (0, 0, 0) in parametric coordinates. These center-point values represent the simple numerical average of the computed Gauss point values.

The material model utilized in this work consists of a simple linear elastic, isotropic material with elastic modulus, $E = 30,000$ ksi and Poisson ratio, $\upsilon = 0.3$. Choice of the linear elastic material model is essentially mandated by the following considerations. Since one of the primary goals of this research is to formulate a method for quantifying the effects of residual stress on the stress intensity factor, K, it is required that large scale plasticity be omitted from consideration. If plasticity were to be included, two major complicating factors would immediately arise. First, it has been widely documented [52-57] that yielding effects can decrease the magnitude of an initial residual stress distribution, sometimes to the point of its complete annihilation. In order to capture such a history dependent phenomenon, cycle by cycle finite element analysis would need to be carried

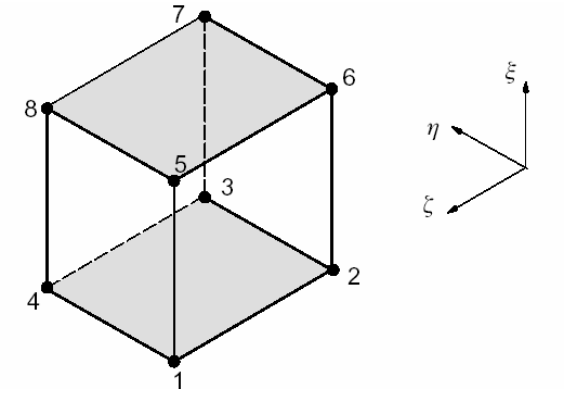

Figure 6.2: Location of Integration Points in Parametric Coordinates: 8-Node Brick Element [51]

Table 6.1: Isoparametric Nodal Coordinates

Node	ξ	η	ζ
1	-1	-1	1
2	-1	-1	-1
3	-1	1	-1
4	-1	1	1
5	1	-1	1
6	1	-1	-1
7	1	1	-1
8	1	1	1

out for each loading scenario considered. This would, in essence, render the task infeasible, since it can sometimes require thousands of load cycles to significantly grow a crack, even under large strain loading conditions. Second is the numerical complication and theoretical uncertainty of going from a K-based description of fatigue to a J-based characterization. Dowling and Begley [58] have applied J-integral concepts to fatigue crack propagation under large scale yielding by fitting crack growth data to a power-law form of ΔJ. Despite their apparent success in developing an empirical relationship, the theoretical basis for such an approach would seem to violate the fundamental principle of similitude, since two structures, cyclically loaded at the same ΔJ, will not exhibit the same crack growth rates unless both structures have undergone the same (plastic) loading history. Furthermore, the deformation plasticity model (nonlinear elasticity), which constitutes the underpinnings of J integral theory, is violated for cyclic loading conditions, since the material, upon unloading, does not behave according to the model.

Model loading consists of two types; applied mechanical load and thermal load (to simulate residual stress). Applied mechanical loading is modeled as both load control and displacement control. As will be shown in Chapter 7, these two loading scenarios can result in different K_{res} solutions. Under load-controlled conditions, the residual stresses can redistribute in a more unrestrained fashion, since there is no nodal displacement constraint, other than the imposed plane strain conditions and symmetry plane constraints. This, essentially free, redistribution of residual stresses generally results in a situation where the residual stress tends to redistribute away from the crack tip. This effect can mean that a growing crack will

experience, for example, a tensile residual stress, even in a region where compressive residual stress initially existed. Displacement-control loading is modeled in this research as well, because it may be more applicable in certain situations. For example, a structural member is typically not free to distort and/or warp to accommodate redistributing residual stresses because it is spatially constrained by adjoining members. Under these conditions, the prediction of fatigue life may be more suitably conducted using the K_{res} values computed from displacement-controlled modeling. The two modeling scenarios, load and displacement control, require a subtle difference in interpretation of the finite element output data. Consider that the potential energy of an elastic body, Π, is given by

$$\Pi = U - F \tag{6.5}$$

where U is the stored strain energy and F is the work done by external forces. Under displacement control conditions, the situation is fairly straight-forward, since $F = 0$, and $\Pi = U$. The energy release rate can be easily calculated by equation (2.21). Under load control however, the situation is more complex. Under normal load-control conditions, without any residual stress being present, the work done by external loading is simply

$$F = P\Delta \tag{6.6}$$

where Δ is the displacement associated with the external loading. Since U in this case, is given by

$$U = \int_0^{\Delta} \frac{1}{2} P d\Delta = \frac{P\Delta}{2} \tag{6.7}$$

the calculation of potential energy change is again straight-forward.

Inclusion of residual stress however, means that as the crack grows, the body will experience displacement at the nodes where external loads are applied, not only due to the applied loading, but also because of the redistributing residual stress. This complication means that knowledge of *both* internal strain energy and external work are required to calculate K_{res} via the load-control method. A precise method for calculating the work done by the external load due to residual stress redistribution is to evaluate the nodal displacements of those nodes where external loading is defined. The net amount of work done by the external loads is then

$$F = \sum_i P_i \Delta_i \tag{6.8}$$

where P_i are the nodal loads and Δ_i are the corresponding nodal displacements. It is required, then, that for each crack increment, a calculation of F be carried out using equation (6.8). Given numerical values for F, it is then possible to calculate the potential energy at each crack increment, thus enabling determination of K_{res}.

Thermal loads, as previously mentioned, are introduced via a spatial distribution of thermal expansion coefficients, such that they simulate residual stresses. In order to isolate strain energy changes related specifically to the mode I stress intensity factor, K_I, only thermal expansion coefficients in the loading direction, α_{yy}, are used. If thermal expansion coefficients other than those representing directions normal to the crack plane are used, the resulting calculation of stress intensity factor will be confounded by multiple mode effects. As a final note concerning the model loading, it must be pointed out that the applied mechanical loading, for purposes of determining K_{res}, must be large enough to result in a total stress

distribution that is positive (tensile) at all points along the crack plane. The reason for this requirement is that a compressive net stress will contribute to strain energy changes with crack growth the same as a tensile net stress, possibly resulting in the erroneous conclusion that even though the stress is compressive, there is a positive K_{res} associated with it.

The steps involved in the actual analysis procedure are broken down into two general categories; those performed only once, and those repeated for each residual stress pattern. These steps are sequenced as follows:

<u>One-time Procedures</u>

- Run progressive mesh refinement on model with mechanical loading only until K-solutions are calibrated to known solution
- Run crack growth analyses for mechanical loading only, obtaining K_{app} as a function of a/W.

<u>Procedures for each Residual Stress</u>

- Add thermal loading and run single step analysis to validate residual stress distribution
- Run crack growth analyses for mechanical loading and thermal loading, obtaining K_{tot} as a function of a/W
- Calculate $K_{res} = K_{tot} - K_{app}$, as a function of a/W

6.2.2 Regression Analysis

On occasion, it has been necessary to perform regression analysis on numerical results in order to establish closed form approximations to those results. This has been necessary, for example, when calculating the weight function solution for a modeled residual stress distribution. The residual stress is known numerically at each element integration point, but the calculation of a weight function solution is sometimes more easily performed by direct integration of a closed form expression for the stress distribution, $\sigma(x)$. In all cases of regression analysis, standard least squares methods are used, and the software utilized is Matlab.

6.2.3 Fatigue Life Predictions

Fatigue life calculations in this research have been carried out using a cycle by cycle procedure implemented with Matlab software. A flow diagram for the cyclic procedure is given in figure 6.3. The basis for the calculation of fatigue life is given by the Forman equation (3.13), given here again for convenience.

$$\frac{da}{dN} = \frac{C\Delta K^m}{(1-R)(K_{crit} - K_{\max})}$$

Input arguments for the program are the initial and final crack lengths, minimum applied stress intensity factor, load range, critical SIF, a column vector consisting of the coefficients of the polynomial fit of K_{res}, threshold SIF range (ΔK_{th}) and the fatigue law material-specific parameters C and m. This program first calculates the effective SIF range, ΔK_{eff}, by superposition of K_{res} and K_{app}. The load ratio, R, is also calculated as

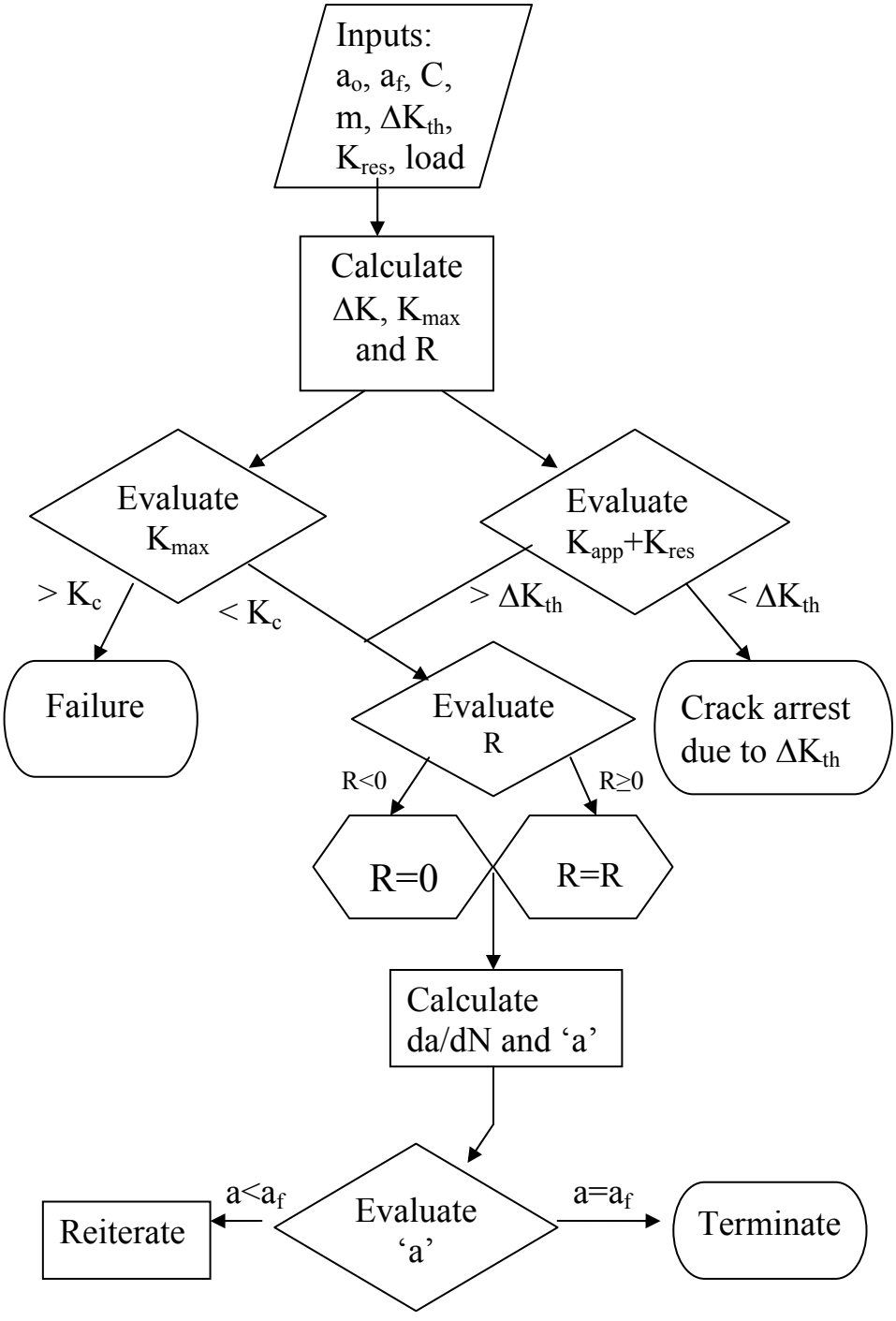

Figure 6.3: Matlab Fatigue Algorithm Flowchart

$$R = \frac{K_{\min\_applied} + K_{res}}{K_{\max\_applied} + K_{res}} \tag{6.9}$$

Note the possibility of obtaining a negative value of R when a compressive residual stress field results in $K_{min\_applied} + K_{res} < 0$. In this case, the value of R is set to zero, and the effect of K_{res} enters the calculation solely through its effect on K_{max} in equation (3.13), where

$$K_{\max} = K_{\max\_applied} + K_{res} \tag{6.10}$$

The possibility also exists for the denominator of equation (6.9) to be less than or equal to ΔK_{th} at some point during the crack growth, in which case the calculation terminates with crack arrest. If neither of the two above cases presents itself, the calculation of crack extension proceeds via equation (3.13) with $dN = 1$, the crack length is updated, and the procedure reiterates until the final desired crack length, or the critical SIF, is reached. Note that this choice of fatigue law, coupled with a cycle by cycle analysis, provides the opportunity to incorporate the effect of K_{res} through both R and K_{max}. Moreover, this coupling accounts for the accelerated crack growth rates evident in Region III of the fatigue crack growth curve (figure 1), and allows for a threshold value lower limit on ΔK. While other, empirically-derived, fatigue laws exist, some of which may be applicable in a modified form or when implemented in a cycle by cycle analysis, this particular choice is justified by the aforementioned advantages.

Chapter 7

Results

The results of this research will be presented as follows. First, the FEM calibration is presented for both plane strain and plane stress states of the SENT specimen. Following the FEM calibration results, a general comparison of weight function vs. energy methods is presented and a detailed explanation of the inherent differences is given. Next are the analyses of individual residual stress patterns. Individual residual stress patterns investigated in this research adhere to one of three general categories. The categories include two resulting from welding and one from shot peening. Each general category is described in subsequent sections, along with a presentation of its analysis results.

7.1 Model Calibration

Model calibration was conducted to establish the maximum mesh size that could be used while maintaining an acceptable level of accuracy. Calculations of the SIF for the SENT geometry were made using the changes in potential energy as determined through FEA. The FEA results were then compared to the non-dimensional master calibration for the SENT geometry. A pre-determined accuracy of +/- 3% was established as the minimum requirement. After several iterations of mesh refinement, it was determined that a mesh size of $\Delta_h / W = 0.025$ provided the desired accuracy, where Δ_h is the actual mesh dimension in the crack growth direction. Figure 7.1 shows the results of the calibration calculations. As

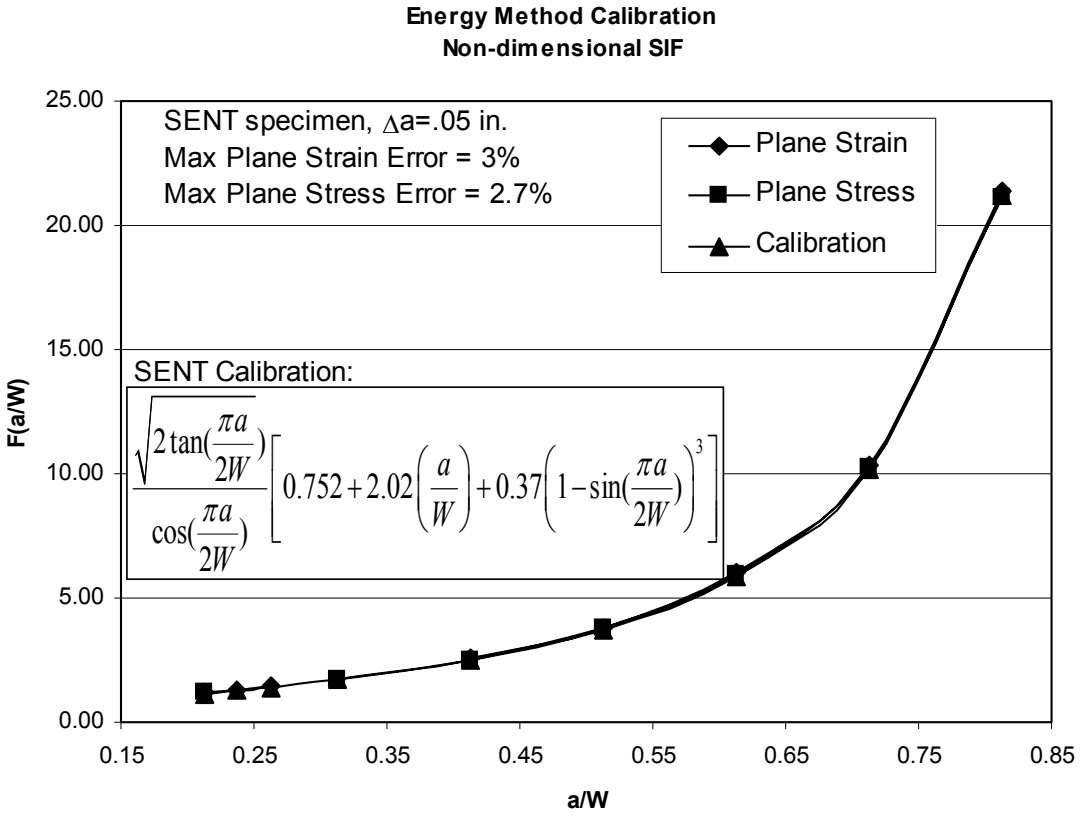

Figure 7.1: Finite Element Model Calibration Results

can be seen from the graph, the model gives very accurate results at the chosen mesh size, and the results have a maximum error of 3 % for plane strain and 2.7 % for plane stress. Note that this error is evaluated at discrete points and does not reflect the possible magnitude of error that may be encountered via an interpolation of these data.

7.2 Energy vs. Weight Function Method

One important goal in this research has been to evaluate the error potential of using weight function methods when dealing with residual stresses and fatigue crack growth. Weight functions were briefly discussed in Chapter 5, and it was therein stated that, given a known residual stress distribution, the SIF for that residual stress could be calculated via equation (5.6). $h(c,a)$, known as the weight function, represents the SIF (per unit thickness) at the crack tip due to a point load at position c along the crack perimeter. The weight function for a finite width, edge-cracked plate can be obtained from figure 7.2. Note that the K-solution in the figure is the SIF for equal and opposite point loads on the crack face. This solution, by definition, is the weight function, if the load is a unit load (P=1). This weight function solution was used to calculate the SIF due to residual stress, and compared to the SIF obtained through energy methods, as described in this research. The residual stress chosen for this comparison is shown in figure 7.3. This residual stress pattern, for purposes of illustration, can be assumed to be a realistic two-dimensional representation of residual stress which can arise via means previously discussed. By expressing the residual stress in figure 7.3 as a function of the parameter c, illustrated in figure 7.2, multiplying this

$$K_I = \frac{2P}{\sqrt{\pi a}} \cdot \frac{G\left(\frac{c}{a}, \frac{a}{b}\right)}{\left(1-\frac{a}{b}\right)^{3/2}\sqrt{1-\left(\frac{c}{a}\right)^2}}$$

$$G\left(\frac{c}{a}, \frac{a}{b}\right) = g_1\left(\frac{a}{b}\right) + g_2\left(\frac{a}{b}\right)\cdot\frac{c}{a} + g_3\left(\frac{a}{b}\right)\cdot\left(\frac{c}{a}\right)^2 + g_4\left(\frac{a}{b}\right)\cdot\left(\frac{c}{a}\right)^3$$

$$g_1\left(\frac{a}{b}\right) = .46 + 3.06\frac{a}{b} + .84\left(1-\frac{a}{b}\right)^5 + .66\left(\frac{a}{b}\right)^2\left(1-\frac{a}{b}\right)^3$$

$$g_2\left(\frac{a}{b}\right) = -3.52\left(\frac{a}{b}\right)^2$$

$$g_3\left(\frac{a}{b}\right) = 6.17 - 28.22\frac{a}{b} + 34.54\left(\frac{a}{b}\right)^2 - 14.39\left(\frac{a}{b}\right)^3 - \left(1-\frac{a}{b}\right)^{3/2} - 5.88\left(1-\frac{a}{b}\right)^5 - 2.64\left(\frac{a}{b}\right)^2\left(1-\frac{a}{b}\right)^3$$

$$g_4\left(\frac{a}{b}\right) = -6.63 + 25.16\frac{a}{b} - 31.04\left(\frac{a}{b}\right)^2 + 14.41\left(\frac{a}{b}\right)^3 + 2\left(1-\frac{a}{b}\right)^{3/2} + 5.04\left(1-\frac{a}{b}\right)^5 + 1.98\left(\frac{a}{b}\right)^2\left(1-\frac{a}{b}\right)^2$$

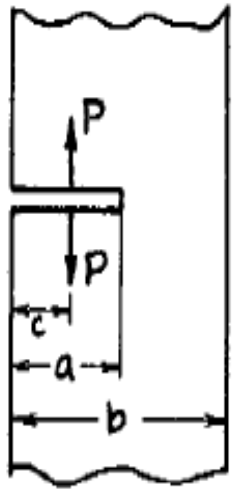

Figure 7.2: Tada Weight Function Solution [10]

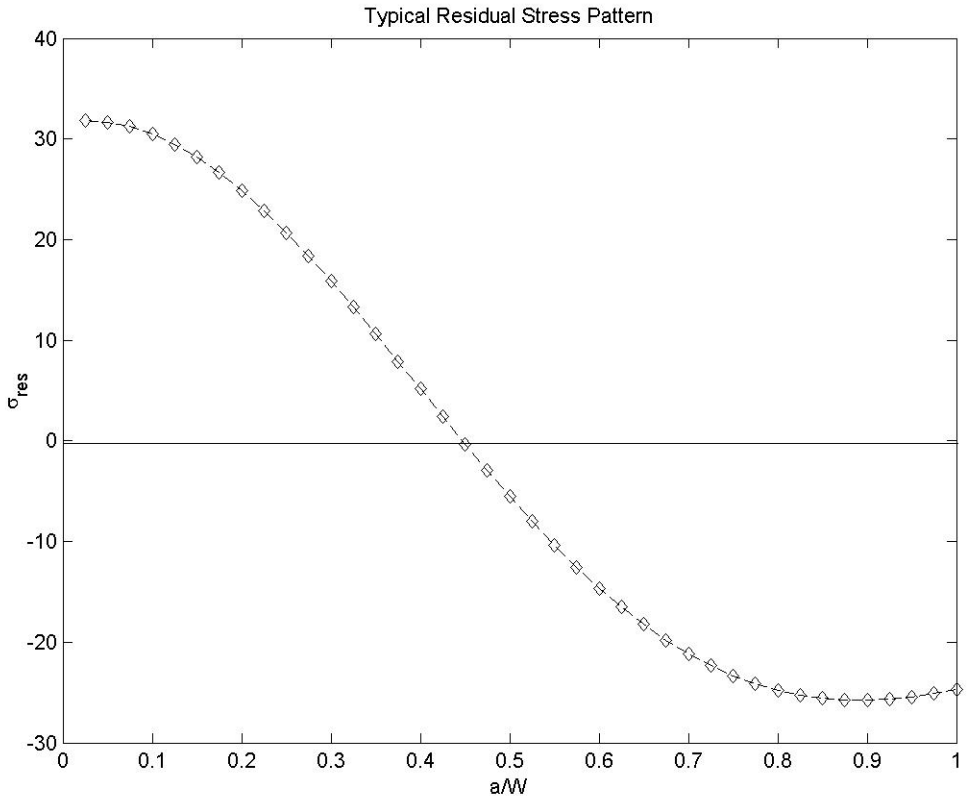

Figure 7.3: Residual Stress Used in Weight Function Analysis

expression by the weight function given in figure 7.2, and integrating as

$$K_{res}(a) = \int_0^a \sigma(c)h(c,a)dc \tag{6.11}$$

a closed form expression for K_{res} can be obtained. Since this closed form solution can be very complicated and difficult to handle, even with advanced computing software such as Matlab and Mathematica, an alternate, numerical integration was employed. To obtain a simpler representation of the solution to equation (7.1), the crack length ratio, a/W, was set at values ranging from 0.05 to 0.65, and numerical integration was then carried out over the variable 'c'. The result of this step-wise numerical integration, and subsequent polynomial regression, is provided in figure 7.4. Comparison of figures 7.3 and 7.4 reveals a rather surprising result. The residual stress becomes compressive somewhere around a/W=0.5, yet the weight function solution for K_{res} remains positive and, in fact, grows exponentially. While a negative SIF has no real physical meaning, it is expected that, for the method of linear superposition of SIF's, K_{res} *must* be negative in a compressive residual stress field. The answer, as to why the weight function approach does not meet this basic requirement, lies in one of the method's fundamental assumptions - that the loading scenario being evaluated does not change with crack growth. From equation (7.1) and figure 7.2, it is clear that the weight function method requires that the stress on an uncracked member be replaced with an equivalent crack face loading, as the crack passes through the member. Since any external loading, by the principle of superposition, can be equally represented with a traction applied directly to

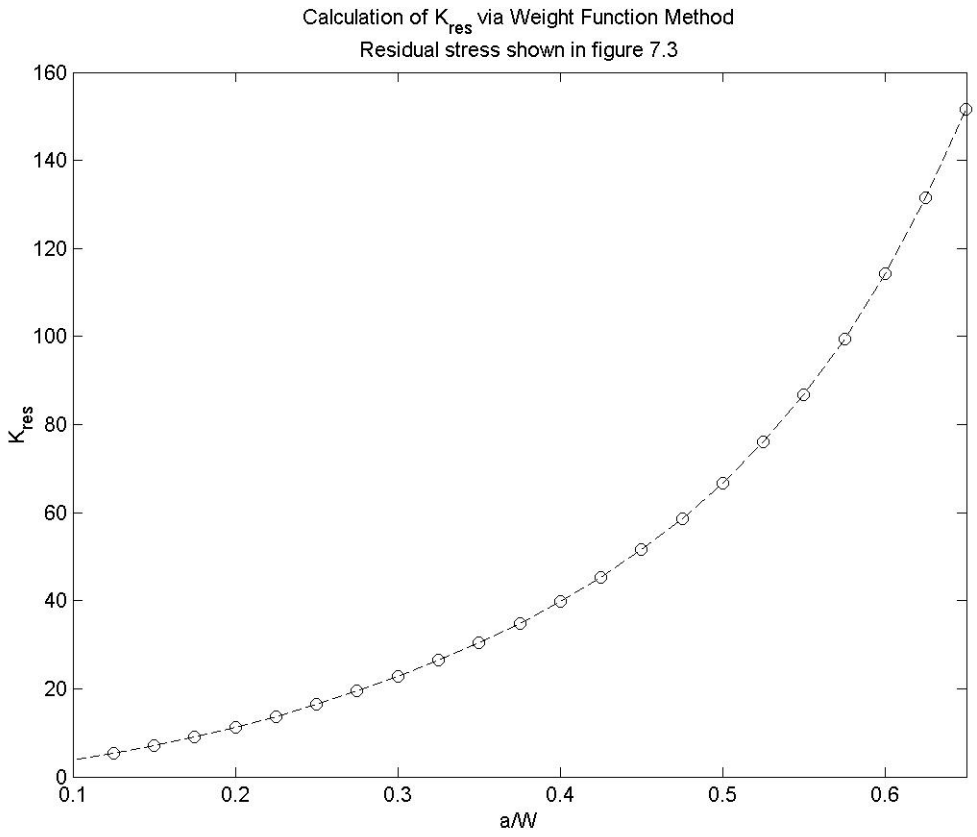

Figure 7.4: K_{res} Calculated Via Weight Function Method

the crack face, the aforementioned assumption, when made in the case of external loading, seems quite reasonable. Making this assumption, however, in the case of a residual stress, would appear to be troublesome for the following reason: the residual stress does, in fact, change as the crack grows. This is easily realized by noting that the stress acting on the crack plane before the crack passes must be zero after the crack tip has passed. The crack plane, now a free surface, must be free of any normal stress, absent an applied crack-face load. With the weight function approach, however, the residual stress which once resided on the uncracked plane, but which has been annihilated by the growing crack, is still given weight as though it were acting on the crack face. Moreover, the crack face loading is taken to be only that part of the residual stress which was acting on the current crack faces before the crack grew to its current size. The remaining residual stress, acting on the uncracked ligament, is ignored. Figure 7.5 illustrates how the weight function gives weight to crack face loadings, even in their apparent absence. Note that in this figure, $0 \le c < a$, where c is defined as in figure 7.2. It can be seen in figure 7.5, for example, that for the SENT geometry, a unit load at $c = 0$ results in a SIF of approximately 3.3 at the crack tip. This is to be expected since those loadings furthest away provide the largest bending stress at the crack tip. Figure 7.5 also illustrates why the K_{res} solution, calculated via the weight function method, remains positive even in the presence of the compressive stress field. The large "weight" given to the loading furthest from the crack tip, which happens to be tensile in this case, dominates any loading due to the compressive region, which is nearer. It would appear that these characteristics of the weight function, giving weight to loadings based on the

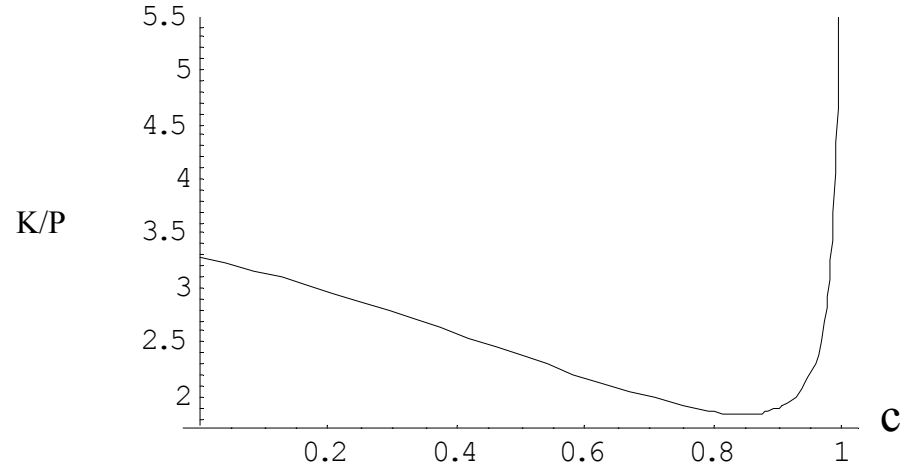

Figure 7.5: SENT Weight Function for a/W=0.5

initial, uncracked stress distribution, and of considering only that part of the residual stress which is behind the crack tip, disqualify it as a plausible method of evaluating the SIF due to a residual stress in the presence of a growing crack. Given the proposition that weight functions may be inappropriate in the evaluation of fatigue crack growth problems involving residual stress, it is interesting to consider what the potential impacts of their use could be. To illustrate those possibilities, fatigue lives were calculated, using the aforementioned Matlab program, for multiple scenarios. Calculations were performed for both the weight function solution of K_{res} (Fig. 7.4) and the energy method solution of K_{res} under displacement control (Figure 7.6). Table 7.1 contains the results of those calculations, where it is evident that fatigue life estimates based on weight function methods result in non-conservative life estimates. For example, using a cyclic load of 5 ksi and an initial crack of 0.1 inches, the weight function predicts over a half million cycles required to grow the crack by 0.5 inches, while the energy

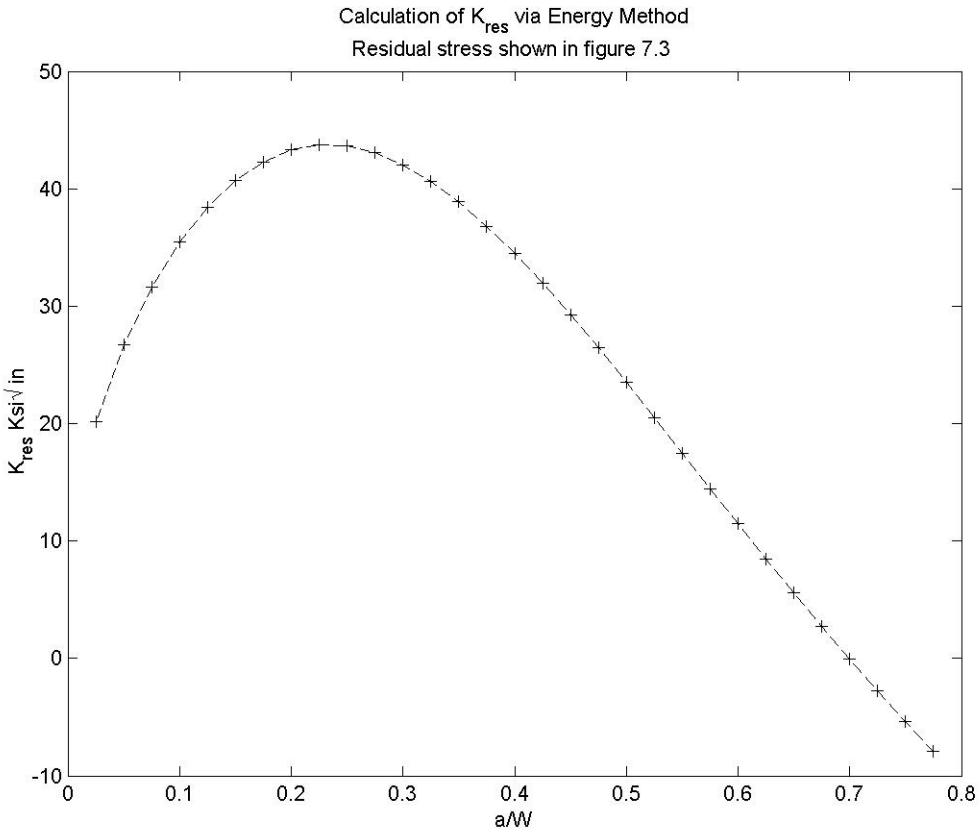

Figure 7.6: K_{res} Calculated via Energy Method

Table 7.1: Fatigue Life Comparison--Energy vs. Weight Function

Fatigue Life Comparisons				
ΔP (ksi)	a_0 (in.)	a_f (in.)	N_f (Energy)	N_f (Weight Function)
5	0.1	0.4	131,340	545,340
10	0.1	0.4	28,850	88,380
15	0.1	0.4	10,359	28,068
5	0.1	0.6	148,580	588,030
10	0.1	0.6	31,516	94,830
15	0.1	0.6	10,869	29,705
5	0.1	0.8	156,009	598,186
3	0.5	1.5	failure	68,478

solution predicts that less than 150,000 are required. In the following section, which describes specific residual stress fields and their effects on K, the corresponding weight function solution is not given. The sole intent of presenting the weight function solution for the above residual stress field is to illustrate the discrepancy between that method and that of the energy approach. Given that discrepancy, and a firm understanding of its origins, subsequent discussion of weight functions is forgone.

7.3 Analysis of Residual Stress Patterns

7.3.1 Welding Residual Stress

The first residual stress pattern to be investigated is one proposed by Masubuchi and Martin [47]. A mathematical representation of this residual stress is given by equation (5.7). Masubuchi and Martin proposed that this pattern represented that typical of the longitudinal residual stress created along a direction perpendicular to a weld bead, as illustrated in figure 7.7.

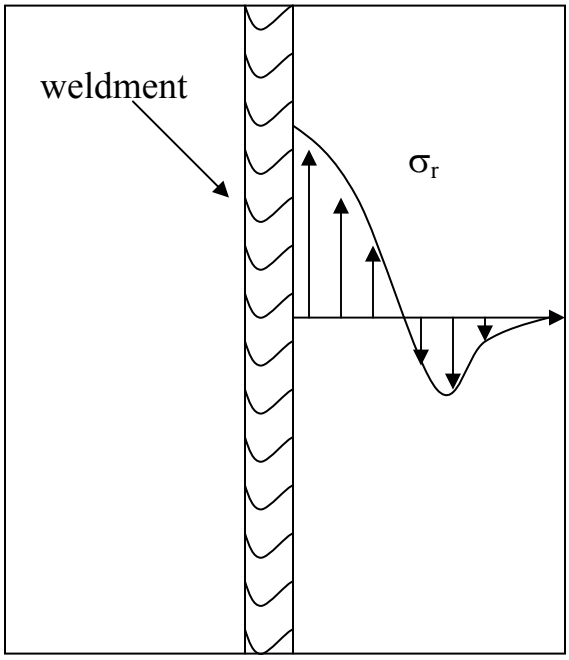

Figure 7.7: Masubuchi Residual Stress (schematic)

Finite element modeling of this residual stress produced the pattern in figure 7.8. Figure 7.9 shows the results of K_{res} calculations based on modeling both a load-control and a displacement-control scenario with this residual stress. It is clear from these results that K_{res} modeled via displacement control is generally larger in magnitude than K_{res} modeled via load control, when considering the entire range or values for a/W. The physical explanation for this is found by investigation of the stress redistribution with crack growth for the two models. Figure 7.10 shows the residual stress distributions after the crack has grown to a/W=0.175. The residual stress for the load-control scenario has redistributed more than for the displacement-control. The net result is that the crack tip stress under load-control is initially higher, resulting in a higher K_{res}. Very quickly, however, the relaxation effect, more pronounced in load-control, begins to dominate. This result is not surprising in the sense that residual stress redistribution is normally thought of as a "relaxation" of the overall stress pattern. The suggestion that the redistribution can result in a higher-magnitude SIF than would be seen without redistribution, i.e., the conclusions of Lee et al. [46], would seem to be somewhat in agreement with these results. Lee's results also indicated that non-conservative predictions of fatigue life could result in certain cases where residual stress redistribution is not taken into account. From the findings of this research, it appears that residual stress redistribution with crack growth has the net effect of reducing the magnitude of K_{res}, and, for the case of a tensile residual stress, extending the fatigue life. To get an idea of the effect the redistribution may have, fatigue lives were estimated with both load and displacement control modeling with the Masubuchi residual

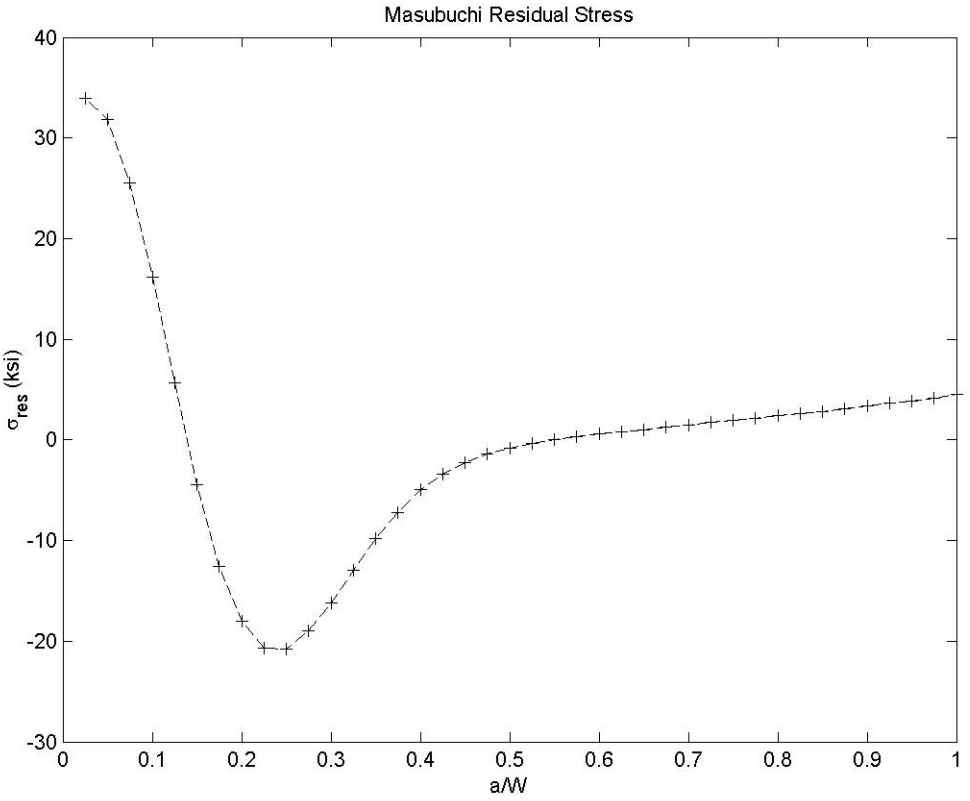

Figure 7.8: Masubuchi Residual Stress (FEA Model)

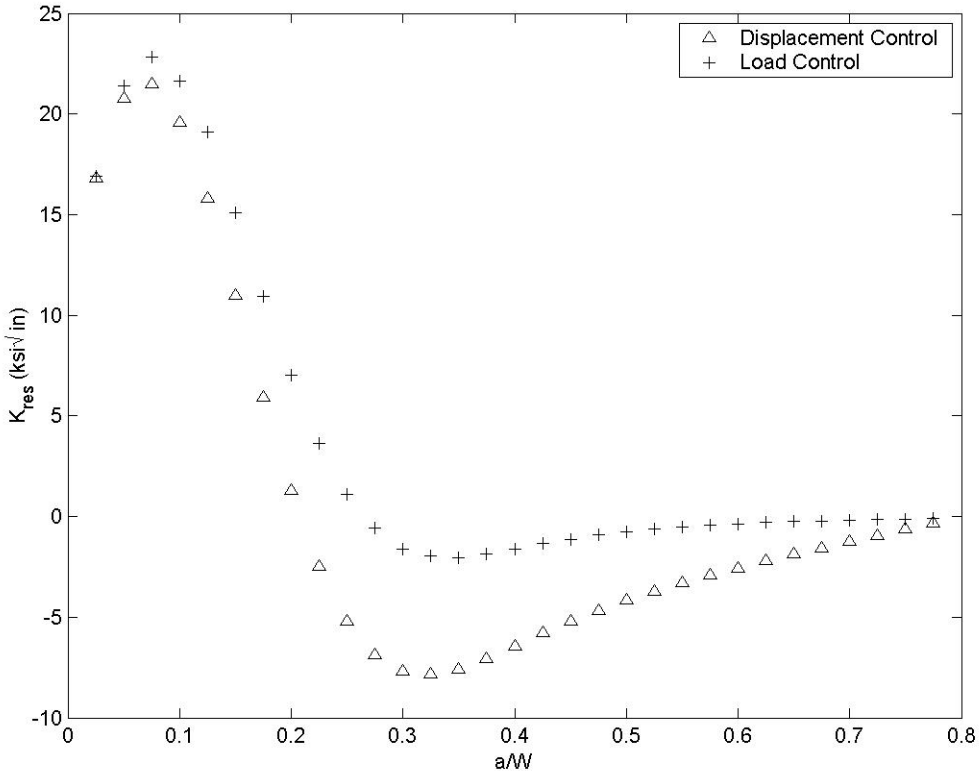

Figure 7.9: Comparison of Load-Control vs. Displacement-Control K_{res} Solutions for Masubuchi Residual Stress

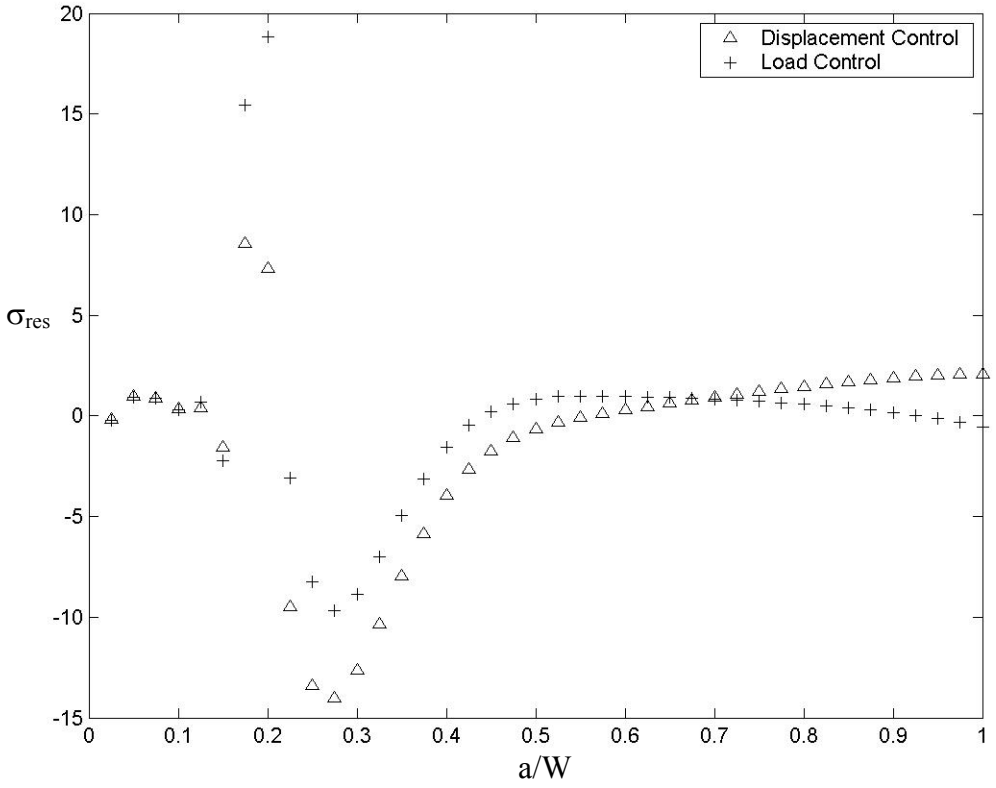

Figure 7.10: Masubuchi Residual Stress Redistribution With Crack Growth

stress and with parameters of $\sigma_r = 35$ ksi and b/W=0.25. The result was an approximate 7% difference in fatigue life, with the load-control model giving the longer predicted life. An interesting and convenient feature of the Masubuchi residual stress pattern, as given by equation (5.7), is that two parameters, σ_r and b, uniquely determine the entire distribution. From equation (5.7), it is clear that σ_r represents the stress amplitude and b represents the x-intercept, or point of zero residual stress, also called the field half-width. By varying these parameters in the FE model, and making subsequent fatigue life predictions, it is possible to infer the trends with each. To investigate these trends, additional models were constructed, and fatigue lives estimated from the K_{res} results. The parameter settings for these models are given in table 7.2, along with the corresponding predicted fatigue lives. These data were fitted to a log-linear regression model to gain an understanding of their trends. The results of the regression are given in table 7.3. From these regression results, it appears that, within the range of the variables considered, fatigue life is significantly influenced by field half-width, but is largely unaffected by stress field amplitude. As a final comment concerning the Masubuchi residual stress pattern, the effect of each of the parameter settings can be compared directly to the value given in table 7.2 for $N_f{}^0$, the predicted fatigue life with no residual stress present. The comparison indicates that the residual stress used in these analyses can reduce the fatigue life by as much as 80%.

A second residual stress pattern that is commonly encountered in welding processes, and which has been documented by Fukuda [48] and

Table 7.2: Parameter Settings and Fatigue Life Predictions for Masubuchi Residual Stress Models (SENT Specimen)

Material: 17-4 PH Steel H1025 N_f^0=35,242			ΔP=20 ksi a_0=0.1 in.
Model #	σ_r (ksi)	b/W	N_f
1	29	0.35	6,904
2	45	0.125	10,301
3	35	0.25	7,631
4	31	0.225	8,103
5	28	0.15	11,499
6	54	0.15	9,701

Table 7.3: Results of Regression on Data from Table 7.2

R^2= 0.9			
Term	Estimate	Std Error	Prob>|t|
Intercept	9.81	0.23	<.0001
σ_r	-0.01	0.01	0.29
b/W	-2.49	0.51	0.02

Bose [59] is that shown schematically in figure 7.11. This welding residual stress occurs along a plane through the centerline of the weld bead, and in the direction parallel to the weld path. As can be seen in the figure, the crack tip starts in a narrow compressive field, transitioning into a broader, but less intense, tensile region. This type residual stress pattern has also been documented by Bose as significantly increasing that part of fatigue life consisting of fatigue crack propagation. Finite element modeling of this residual stress produced the pattern in figure 7.12. Figure 7.13 shows the results of K_{res} calculations based on modeling both a load-control and a displacement-control scenario with this residual stress. It is evident from figure 7.13 that the redistribution effect, more pronounced in the load-control model, has resulted in a lower K_{res} result across almost the entire range of a/W values. In this case, and similarly to the Masubuchi pattern already discussed, the magnitude of K_{res} is generally less for load control vs. displacement control. Also in this case, the effect of K_{res} will initially be much greater for load control than for displacement control. This result can be explained by referring to figure 7.14, which shows how the residual stress redistributes with crack growth. From this figure, it can be seen that the residual stress is tending to redistribute away from the crack tip, resulting in a higher magnitude of crack tip stress vs. that of no redistribution. This result agrees closely with that of Fukuda [48], concerning the redistribution behavior of this particular residual stress pattern in the presence of a growing crack. To gain an appreciation of what this redistribution effect would mean in terms of fatigue life, predictions were made with the Matlab program using the same material properties as with the Masubuchi predictions. The results of the fatigue life calculations

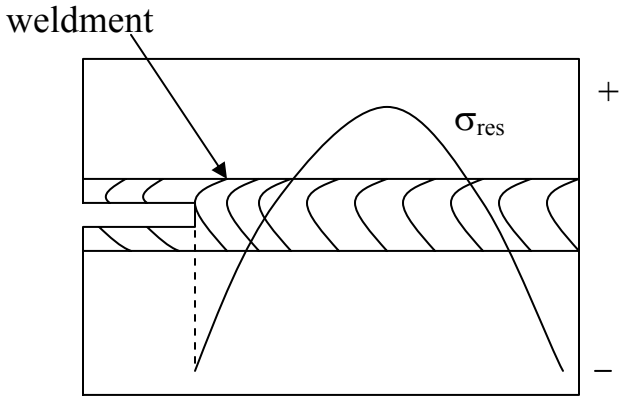

Figure 7.11: Parabolic Welding Residual Stress Pattern

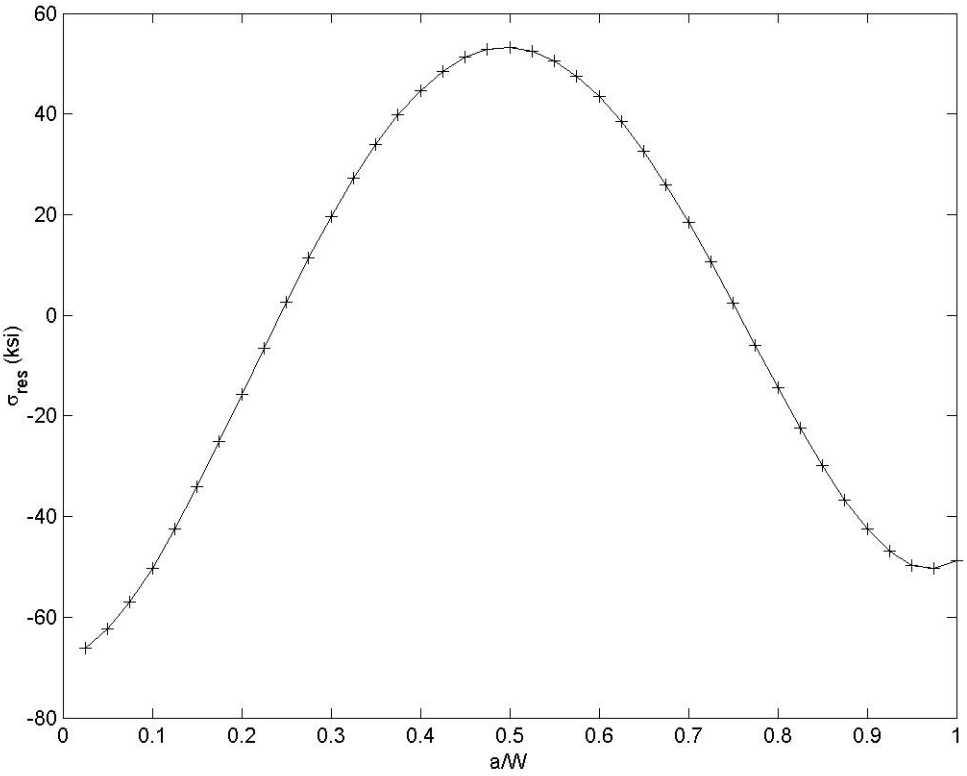

Figure 7.12: Parabolic Welding Residual Stress (FEA Model)

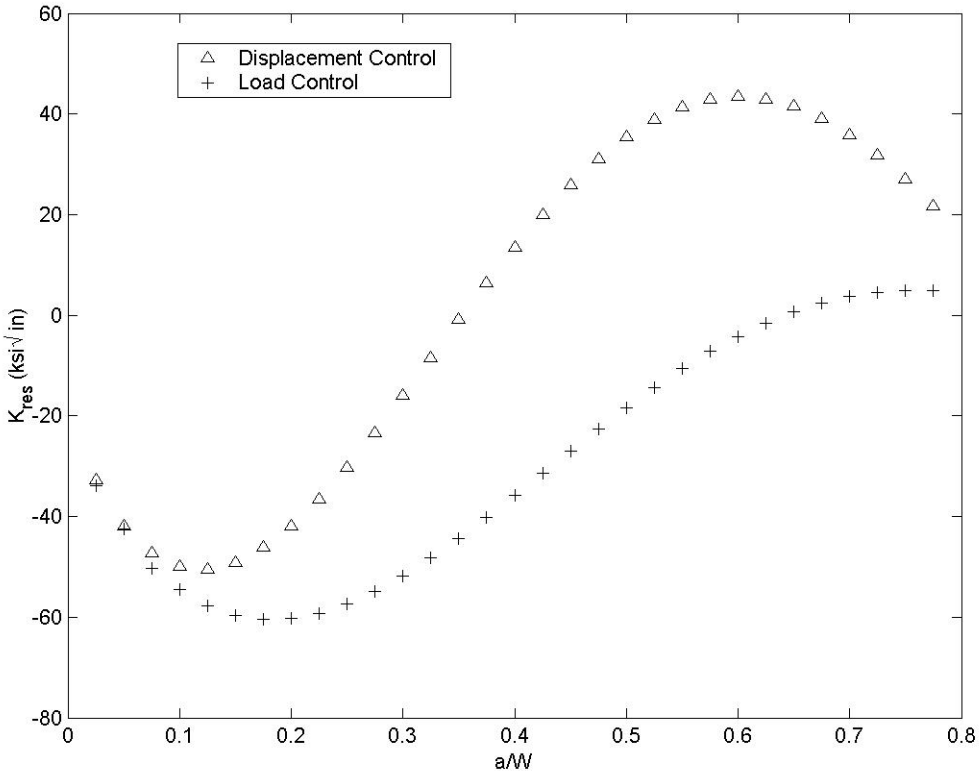

Figure 7.13: Comparison of Load-Control vs. Displacement-Control K_{res} Solutions for Parabolic Residual Stress

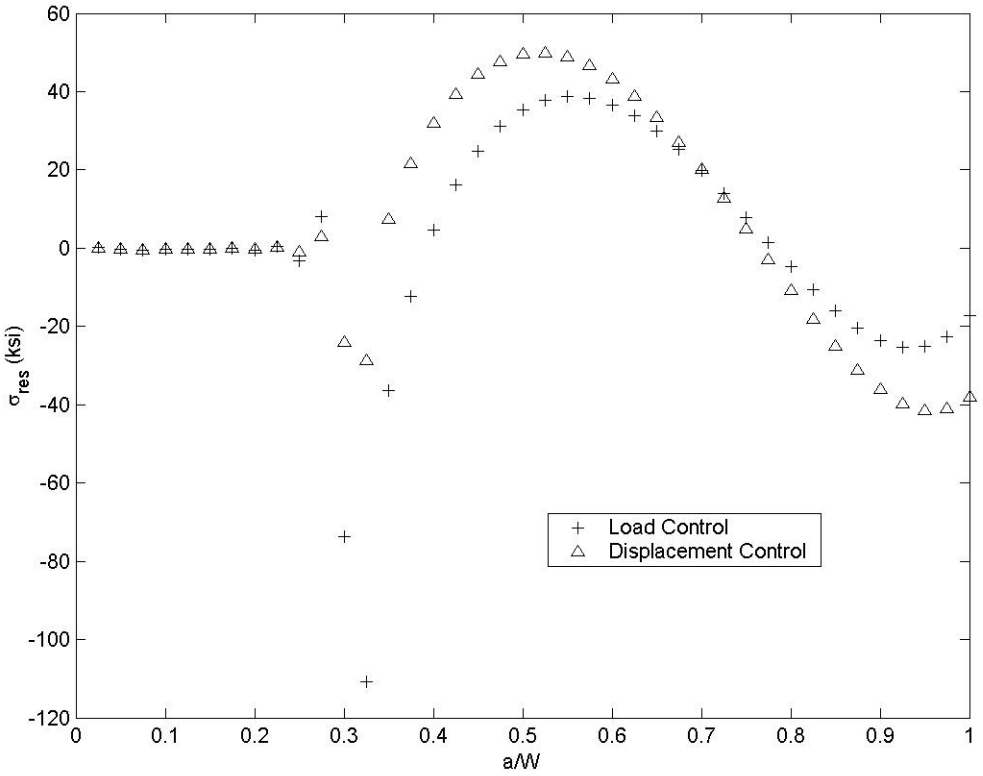

Figure 7.14: Parabolic Residual Stress Redistribution With Crack Growth

for load vs. displacement control are given in table 7.4. Again, the difference, in terms of fatigue life in this example, is approximately 7% and again, the load-control model gives the longer fatigue life. Also note that the presence of the residual stress extends fatigue life to almost twice its life without the presence of residual stress.

7.3.2 Shot Peening Residual Stress

As previously discussed in the chapter on residual stress formation, plastic deformation will typically introduce a residual stress when material surrounding a yielded zone attempts to elastically recover. One example of a residual stress induced by plastic deformation is that of shot peening residual stress. The process of shot peening involves blasting the surface of a component with hard, spherical, steel or glass shot. The impact of these objects with the surface creates small plastic deformation zones, which become somewhat compressed by the adjacent elastic material. The net result of this process is a thin layer of compressive residual stress near the surface of the component. These shot peening residual stress patterns have been documented by Zhuang [53], Gurova [60], Lu [61], Torres [62] and

Table 7.4: Fatigue Life Predictions for Parabolic Residual Stress Models (SENT Specimen)

Material: 17-4 PH Steel H1025 N_f^0=3,327	ΔP=30 ksi a_0=0.1 in.
N_f (Load Control)	N_f (Displacement Control)
6,438	5,943

others. Figure 7.15 shows the results of finite element modeling of this residual stress pattern. In general, introduction of this type of residual stress pattern through shot peening is intended to extend fatigue life via the delay of crack initiation. It is interesting however, to consider what effect this pattern has on that part of the fatigue life remaining after the crack has initiated and begins to grow. To investigate that question, K_{res} computations were made with both load and displacement-controlled models. The results of those computations are presented in figure 7.16. Again, while the two methods yield similar initial results, the solutions begin to diverge for greater crack lengths. Fatigue life calculations are given in table 7.5 for the two modeling scenarios as well as the predicted life without residual stress. In this case, the difference between using load control vs. a displacement-control model is approximately 3%, with the load-control model predicting the longer life. It should also be noted that the residual stress of figure 7.15 is predicted to extend the fatigue life, under these conditions, by almost 22%.

As with the Masubuchi residual stress pattern, the shot peening pattern can be completely characterized (in two dimensions) by two variables, the compressive field half-width, b/W, and the stress amplitude, σ_r. In fact, for modeling purposes, the shot peening residual stress of figure 7.15 can be generated by inverting the Masubuchi pattern in figure 7.8. To investigate the effect of the above-mentioned variables on fatigue life prediction, the fatigue lives shown in table 7.6 were computed. These data were then used to construct a log-linear model relating predicted fatigue life, N_f, to the field half-width and stress amplitude. The results of this

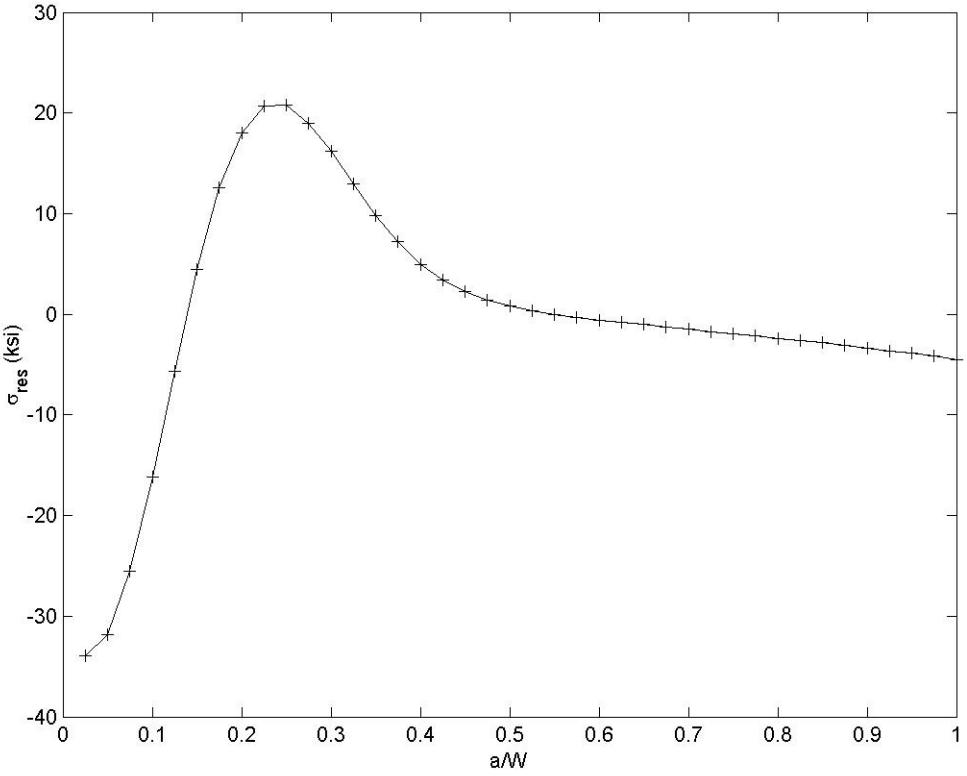

Figure 7.15: Shot Peening Residual Stress (FEA model)

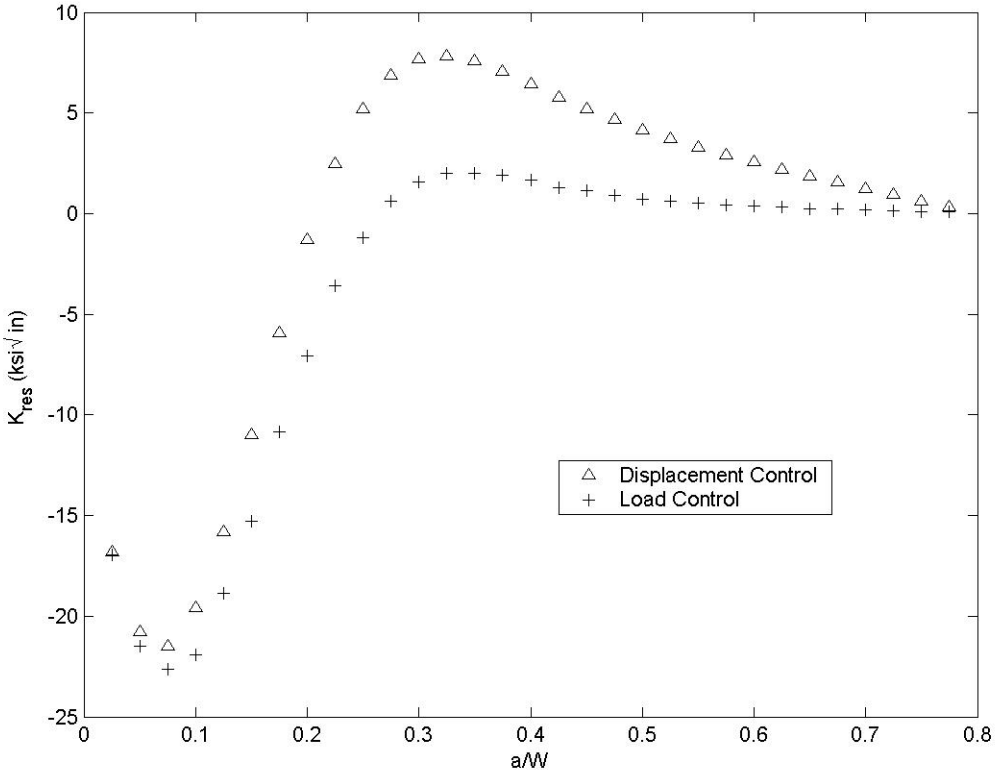

Figure 7.16: Comparison of Load-Control vs. Displacement-Control K_{res} Solutions for Shot Peening Residual Stress

Table 7.5: Fatigue Life Predictions for Shot Peening Residual Stress Models (SENT Specimen)

Material: 17-4 PH Steel H1025 N_f^0=14,328	ΔP=20 ksi a_0=0.1 in.
N_f (Load Control)	N_f (Displacement Control)
17,154	16,647

Table 7.6: Parameter Settings and Fatigue Life Predictions for Shot Peening Residual Stress Models (SENT Specimen)

Material: 17-4 PH Steel H1025 N_f^0=14,328			ΔP=20 ksi a_0=0.1 in.
Model #	σ_r (ksi)	b/W	N_f
1	-34	0.25	17,154
2	-30	0.225	16,184
3	-45	0.125	15,522
4	-27	0.15	14,913
5	-54	0.15	15,835
6	-28	0.35	17,854

regression are given in table 7.7. Again, the regression indicates that, within the range of the variables considered, predicted fatigue life depends on field half-width, but is essentially independent of stress amplitude. This would indicate that stress amplitude, while an important factor in delaying crack initiation, if not large enough to immediately arrest an initial crack, may have a much lesser effect on the remaining fatigue life.

Table 7.7: Results of Regression on Data from Table 7.6

R^2= 0.91			
Term	Estimate	Std Error	Prob>|t|
Intercept	9.45	0.07	<.0001
σ_r	0.00	0.00	0.25
b/W	0.87	0.17	0.01

Chapter 8

Conclusions and Recommendations

Chapters 6 and 7 have shown that a precise formulation of the stress intensity factor due to the presence of residual stress, K_{res}, is possible. The formulation involves characterization of K_{res} as that part of the total stress intensity that is not due to applied loading, and which can be found through superposition of finite element results. The relationship between G, the change in potential energy of a body with crack extension, sometimes referred to as the crack driving force, and K, the stress intensity factor, is exploited to eliminate the need for intricate crack tip mesh construction and for detailed crack tip stress analysis.

Comparison of this energy method for obtaining K_{res} with that of the weight function method has revealed a very significant discrepancy. The weight function method, while seemingly appropriate for external loading, appears to require at least two inherent assumptions which do not apply to residual stresses. The first of these assumptions is that the residual stress maintains its initial magnitude and distribution throughout the entire crack growth process. This assumption has been shown to be an unfounded one. The residual stress redistributes in several ways which all affect the stress intensity factor. Residual stresses essentially relax to zero behind the crack tip, and tend to redistribute ahead of the crack tip to maintain an equilibrium state. Moreover, there is an overall relaxation of residual stress associated with crack growth which must be taken into account. The second inherent assumption in the use of weight functions for residual stress is that it is sufficient to consider only that part of the residual stress that was acting on

the crack plane up to the current crack tip. This assumption violates one of the fundamental principles which underlies weight function theory, and that is the principle of superposition. For the weight function approach to be legitimate, the crack face loading used must be an *equivalent* crack face loading, providing the same *total* stress distribution as the loading it replaces. To replace a complete residual stress distribution with only a part of that same distribution on the crack face does not meet the equivalence requirement.

Proceeding with the evaluations using energy methods through finite element analysis, it has been shown that there are at least two alternative modeling approaches which can give somewhat different solutions for K_{res}. One method, load control, involves superposition of a residual stress onto a constant-load model. In this model, the redistribution of residual stress was shown to be more pronounced, since there are essentially no displacement constraints other than those imposed on the crack plane, and those for imposition of plane strain conditions. This type of model was shown to require a subtle adjustment in the handling of strain energy results because the change in potential energy with crack extension is no longer equal to the change in internal strain energy, since the external loading does some additional work when the residual stress redistribution causes nodal displacement at externally loaded nodes. The second modeling approach, displacement control, involves superposition of a residual stress onto a fixed-displacement model. In this case, redistribution of residual stress was observably less, and determination of K_{res} more straight-forward. The choice of which method to use should be made with a solid understanding of the physical situation being modeled. Displacement control models may be

more appropriate, for example, when investigating components or structural members which are rigidly constrained, and which may not allow free redistribution of residual stress with crack growth. For the examples investigated in this research, displacement control was also shown to give the more conservative life estimates.

Three residual stress patterns were investigated in order to gain some insight as to their behavior and their effects on fatigue life. The Masubuchi residual stress, which arises under certain welding conditions, was shown to decrease predicted fatigue life for a crack originating in or near the weld zone and propagating perpendicular to the weldment. By varying the parameters of the Masubuchi residual stress, it was also shown that the residual stress field half-width, as defined in equation (5.7), has a significant effect on predicted fatigue life, while the stress amplitude may play a lesser role. Parabolic residual stress patterns, arising under previously described welding conditions, were shown to significantly increase fatigue life prediction due to the compressive stress field initially at the crack tip. Lastly, residual stresses arising from the process of shot peening were shown to increase predicted fatigue life, also due to the presence of a compressive field at the initial crack tip. Similar to the Masubuchi residual stress, the shot peening residual stress parameters were varied, and trends with those parameters examined, indicating again that the field half-width is of primary importance, while the residual stress amplitude may be of less importance.

While the above-mentioned conclusions are significant, much remains to be investigated. Of primary importance would be the extension of this method to three-dimensional residual stress problems. For the case of constant through-thickness residual stress and a through-thickness crack,

calculation of potential energy changes with increase in crack surface area can be managed, albeit with significant effort. To extend the problem in another dimension however, would add a level of complexity to the determination of, for example, incremental crack surface area. Moreover, the stress intensity in the general three-dimensional problem would vary along the crack front and fatigue life calculations would become computationally intensive, having to account for non-uniform crack front growth. While these complications may seem daunting, they are certainly manageable with the computing power of today's average desktop computer.

A second interesting extension of the energy method presented in this research would be to model multiple mode fracture, encompassing modes II and III. The ideas and methods presented thus far were applied only to mode I stress intensity calculations, but would be equally valid when applied to multiple mode situations. Multiple mode modeling however, would require added levels of superposition to avoid the confounding of results. Also, this type analysis implies modeling of multi-dimensional residual stress, which has proven to be extremely tedious, and appears, for the present, to be best accomplished through trial and error.

Lastly, these results, of course, require validation through fatigue testing. The general trends and residual stress effects presented in this research agree with those of previous research, and with intuition. Comparable empirical results however, have not been published. It is important, therefore, that a rigorous validation program be completed if the methods presented in this research are to be further investigated.

Bibliography

Bibliography

[1] Duga, J.J., Fisher, W.H., Buxbaum, R.W., Rosenfield, A.R., Burh, A.R., Honton, E.J., and McMillan, S.C., "The Economic Effects of Fracture in the United States." NBS Special Publication 647-2, United States Dept. of Commerce, Washington, DC, March 1983.

[2] Bannerman, D.B. and Young, R.T., "Some Improvements Resulting from Studies of Welded Ship Failures." Welding Journal, Vol. 25, 1946.

[3] Paris, P.C., Gomez, M.P., and Anderson, W.P., "A Rational Analytic Theory of Fatigue." The Trend in Engineering, Vol. 13, 1961, pp. 9-14.

[4] Paris, P.C. and Erdogan, F., "A Critical Analysis of Crack Propagation Laws." Journal of Basic Engineering, Vol. 85, 1960, pp. 528-534.

[5] Anderson, T.L., "Fracture Mechanics: Fundamentals and Applications," CRC Press, New York, 1995.

[6] Inglis, C.E., "Stresses in a Plate Due to the Presence of Cracks and Sharp Corners." Transactions of the Institute of Naval Architects, Vol. 55, 1913, pp. 219-241.

[7] Westergaard, H.M., "Bearing Pressures and Cracks." Journal of Applied Mechanics, Vol. 6, 1939, pp. 49-53.

[8] Irwin, G.R., "Analysis of Stresses and Strains Near the End of a Crack Traversing a Plate." Journal of Applied Mechanics, Vol. 24, 1957, pp.361-364.

[9] Sneddon, I.N., "The Distribution of Stress in the Neighborhood of a Crack in an Elastic Solid." Proceedings, Royal Society of London, Vol. A-187, 1946, pp. 229-260.

[10] Tada, H., Paris, P.C., and Irwin, G.R., "The Stress Analysis of Cracks Handbook," 2nd Ed. Paris Productions, Inc., St. Louis, 1985.

[11] Baker, A.J., "Notes on n-Dimensional Computational Mechanics", Computational Fluid Dynamics Course, The University of Tennessee-Knoxville, Jan, 2000.

[12] Irwin, G.R., "Onset of Fast Crack Propagation in High Strength Steel and Aluminum Alloys." Sagamore Research Conference Proceedings, Vol. 2, 1956, pp. 289-305.

[13] Rice, J.R., "A Path Independent Integral and the Approximate Analysis of Strain Concentration by Notches and Cracks." Journal of Applied Mechanics, Vol. 35, 1968, pp. 379-386.

[14] E399-90, Standard Test Method for Plain-Strain Fracture Toughness of Metallic Materials, American Society for Testing and Materials, Philadelphia, 1990.

[15] Irwin, G.R., "Plastic Zone Near a Crack and Fracture Toughness." Sagamore Research Conference Proceedings, Vol. 4, 1961.

[16] Dugdale, D.S., "Yielding in Steel Sheets Containing Slits." Journal of the Mechanics and Physics of Solids, Vol. 8, 1960, pp. 100-104.

[17] Barenblatt, G.I., "The Mathematical Theory of Equilibrium Cracks in Brittle Fracture." Advances in Applied Mechanics, Vol. 7, Academic Press, 1962, pp.55-129.

[18] Burdekin, F.M., and Stone, D.E.W., "The Crack Opening Displacement Approach to Fracture Mechanics in Yielding Materials." Journal of Strain Analysis, Vol. 1, 1966, pp. 145-153.

[19] Dowling, N.E., "Mechanical Behavior of Materials," 2nd Edition, Upper Saddle, NJ, Prentice-Hall, Inc., 1999

[20] Foreman, R.G., Keary, V.E., and Engle, R.M., "Numerical Analysis of Crack Propagation in Cyclic-Loaded Structures." Journal of Basic Engineering, Vol. 89, 1967, pp. 459-464.

[21] Walker, K., "The Effect of Stress Ratio during Crack Propagation and Fatigue for 2024-T3 and 7075-T6 Aluminum." Effects of Environment and Complex Load History on Fatigue Life, ASTM STP 462, American Society for Testing and Materials, West-Conshohocken, PA, 1970, pp. 1-14.

[22] Klesnil, M., and Lukas, P., "Influence of Strength and Stress History on Growth and Stabilization of Fatigue Cracks." Engineering Fracture Mechanics, Vol. 4, 1972, pp. 77-92.

[23] McEvily, A.J., "On Closure in Fatigue Crack Growth." ASTM STP 982, American Society for Testing and Materials, Philadelphia, 1988, pp. 35-43.

[24] Elber, W., "Fatigue Crack Closure Under Cyclic Tension." Engineering Fracture Mechanics, Vol. 2, 1970, pp. 37-45.

[25] Suresh, S. and Ritchie, R.O., "Propagation of Short Fatigue Cracks." International Metallurgical Reviews, Vol. 29, 1984, pp. 445-476.

[26] Schijve, J., "Some Formulas for the Crack Opening Stress Level." Engineering Fracture Mechanics, Vol. 14, 1981, pp. 461-465.

[27] Gomez, M.P., Ernst, H., and Vazquez, J., "On the Validity of Elber's Results on Fatigue Crack Closure for 2024-T3 Aluminum." International Journal of Fracture, Vol. 12, 1976, pp. 178-180.

[28] Clerivet, A. and Bathias, C., "Study of Crack Tip Opening Under Cyclic Loading Taking into Account the Environment and R-ratio." Engineering Fracture Mechanics, Vol. 12, 1979, pp. 599-611.

[29] Shih, T.T. and Wei, R.P., "A Study of Crack Closure in Fatigue." Engineering Fracture Mechanics, Vol. 6, 1974, pp. 19-32.

[30] Wheeler, O.E., "Spectrum Loading and Crack Growth." Journal of Basic Engineering, Vol. 94, 1972, pp.181-186.

[31] Newman, J.C., "Prediction of Fatigue Crack Growth Under Variable Amplitude and Spectrum Loading Using a Closure Model." ASTM STP 761, American Society for Testing and Materials, Philadelphia, 1982, pp. 255-277.

[32] Walker, D., "Residual Stress Measurement Techniques." Advanced Materials and Processes, Vol. 159, August 2001, pp. 30-33.

[33] Hill, Michael R., "Determination of Residual Stress Based on the Estimation of Eigenstrain." PhD Dissertation, Stanford University, August 1996.

[34] Pavier, M.J., Poussard, C.G.C., and Smith, D.J., "Finite Element Modeling of the Interaction of Residual Stress with Mechanical Load for a Crack Emanating from a Cold Worked Fastener Hole." Journal of Strain Analysis, Vol. 33, 1998, No. 4, pp.275-289.

[35] O'Dowd, N.P., Lei, Y., and Webster, G.A., "Fracture Mechanics Analysis of a Crack in a Residual Stress Field." International Journal of Fracture, Vol. 106, 2000, pp. 195-216.

[36] Matos, C.G., and Dodds, R.H., Jr., "Modeling the Effects of Residual Stresses on Defects in Welds of Steel Frame Connections." Engineering Structures, Vol. 22, 2000, pp.1103-1120.

[37] Mura, T., "Micromechanics of Defects in Solids." The Netherlands: Kluwer Academy Publishers, 1991.

[38] Ueda, Y. Fukuda, K., "New Measuring Method of Three Dimensional Residual Stress in Long Welded Joints Using Inherent Strains as Parameters-L Method." Journal of Engineering Materials and Technology, Vol. 111, 1987, pp.1-8.

[39] Malvern, L.E., Introduction to the Mechanics of a Continuous Medium. Englewood Cliffs, NJ, Prentice-Hall Publishing, 1969

[40] Hill, M.R., Nelson, D.V., "The Inherent Strain Method for Residual Stress Determination and its Application to a Long Welded Joint." Structural Integrity of Pressure Vessels, Piping, and Components, ASME, 1995, Vol. 318, pp. 343-352.

[41] Galatolo, R., and Lanciotti, A., "Fatigue Crack Propagation in Residual Stress Fields of Welded Plates." International Journal of Fatigue, Vol. 19, 1997, pp. 43-49

[42] Fitzpatrick, M.E. and Edwards, L., "Fatigue Crack/Residual Stress Field Interactions and Their Implications for Damage-Tolerant Design." Journal of Materials Engineering and Performance, Vol. 7(2), 1998, pp. 190-198.

[43] Shi, Y.W., Chen, B.Y. and Zhang, J.X., "Effects of Welding Residual Stresses on Fatigue Crack Growth Behavior in Butt Welds of Pipeline Steel." Engineering Fracture Mechanics, Vol. 36, No. 6, 1990, pp. 893-902.

[44] Nguyen, T.N. and Wahab, M.A., "The Effect of Residual Stresses and Weld Geometry on the Improvement of Fatigue Life." Journal of Materials Processing Technology, Vol. 48, 1995, pp. 581-588.

[45] Beghini, M., Bertini, L. and Vitale, E., "Fatigue Crack Growth in Residual Stress Fields: Experimental Results and Modeling." Fatigue & Fracture of Engineering Materials & Structures, Vol. 17, No. 12, 1994, pp. 1433-1444.

[46] Lee, Yong-Bok, Chung, Chin-Sung, Park, Young-Keun and Kyung, Ho, "Effects of Redistributing Residual Stress on the Fatigue Behavior of SS330 Weldment." International Journal of Fatigue, Vol. 20, No. 8, 1998, pp. 565-573.

[47] Masubuchi, K. and Martin, D.C., "Investigation of Residual Stresses by use of Hydrogen Cracking." Welding Journal, Vol. 40, No. 12, 1961, pp. 553-563.

[48] Fukuda, S., "Analysis of Crack Propagation in a Residual Stress Field Using Computer Algebra." Nuclear Engineering and Design, Vol. 111, 1989, pp. 21-25.

[49] Matlab, Version 5.3, The Math Works, Inc. 1999.

[50] Mathematica, Version 4.0, Wolfram Research, 1996.

[51] Dodds, R.H., Warp3D: 3-D Dynamic Nonlinear Analysis of Fracture in Solids. Structural Research Series (SRS) 596, UILU-ENG-94-2017, University of Illinois at Urbana-Champaign, 2002.

[52] Webster, G.A. and Ezeilo, A.N., "Residual Stress Distributions and Their Influence on Fatigue Lifetimes." International Journal of Fatigue, Volume 23, 2001, pp. 375-383.

[53] Zhuang, W.Z. and Halford, G.R., "Investigation of Residual Stress Relaxation Under Cyclic Load." International Journal of Fatigue, Volume 23, 2001, pp. 31-37.

[54] Mattson, RL and Coleman, WS Jr., "Effect of Shot Peening Variables and Residual Stresses on Fatigue Life of Leaf Spring Specimens." Transactions, Society of Automotive Engineers, Volume 62, 1954, pp. 546-556.

[55] Morrow, J. and Sinclair, G.M., "Cycle-Dependent Stress Relaxation." Symposium on Basic Mechanisms of Fatigue, ASTM STP 237, American Society for Testing and Materials, 1958.

[56] Jhansale, H.R. and Topper, T.H., "Engineering Analysis of the Inelastic Stress Response of a Structural Metal Under Variable Cyclic Strains." Cyclic Stress-Strain Behavior—Analysis, Experimentation and Failure Prediction, American Society for Testing and Materials, 1973, pp. 246-270.

[57] Wallace, W.P. and Frankel, J.P., "Relief of Residual Stresses by Single Fatigue Cycle." Welding Journal, Volume 38, 1949, p. 565.

[58] Dowling, N.E. and Begley, J.A. "Fatigue Crack Growth During Gross Plasticity and the J Integral." ASTM STP 590, American Society for Testing and Materials, Philadelphia, 1976, pp. 82-103.

[59] Bose, W., personal communication, May 2001

[60] Gurova, T., Teodosio, J.R., Monine, V., "Analysis of Residual Stress State in Speed Gears for Automotive Vehicles." Fourth International Workshop on Non-Destructive Testing and Computer Simulations in Science and Engineering, Volume 4348, 2001, pp. 308-311.

[61] Lu, J., "Introduction to the Prestress Engineering Approach." Heat Treating; Advances in Surface Engineering; An International Symposium in Honor of Professor Tom Bell and Professor Tom B. Cohen Memorial, Volume 1, 2000, pp. 382-391.

[62] Torres, M.A., Voorwald, H.J., "An Evaluation of Shot Peening, Residual Stress and Stress Relaxation on the Fatigue Life of AISI 4340 Steel." International Journal of Fatigue, Volume 24, No. 8, 2002, pp. 877-886.

Vita

Jeffrey L. Roberts was born in McMinnville, Tennessee on February 2, 1967. He studied within the Warren County public school system for eleven years before withdrawing enrollment his senior year. He successfully completed the General Education Development (GED) test in 1985 and that year received his high school diploma. He received a Bachelor of Science degree in Engineering Physics from the University of Tennessee in 1992 and a Master of Science degree in Engineering Science in 1999. Since 1995, he has been employed with Saturn Corporation, a division of General Motors. His roles at Saturn have included Dimensional Engineer, Manufacturing Engineer, Product Engineer and, most recently, Statistical Engineer. In 2002, he received the Doctor of Philosophy degree in Engineering Science from the University of Tennessee at Knoxville.